Supporting Information for

Uncovering the Influence of Modifier Redox Potential on CO_2 Reduction through Data-driven Machine Learning and Hypothesis-driven Experimentation

Xinru He,‡[a] Yuming Su,‡[a] Jieyu Zhu,‡[a] Nan Fang,[a] YangTao Chen,[a] Huichong Liu,[a] Da Zhou,*[b] and Cheng Wang*[a]

[a] State Key Laboratory of Physical Chemistry of Solid Surfaces, iChem, Innovation Laboratory for Sciences and Technologies of Energy Materials of Fujian Province (IKKEM), College of Chemistry and Chemical Engineering, Xiamen University, Xiamen 361005, P. R. China.

[b] School of Mathematical Sciences, Xiamen University, Xiamen 361005, China.

Table S1. Comparison of CO_2RR catalytic performance of different type of modified Cu-based electrocatalysts.

Catalysts	Electrolyte	Cell type	E (V *vs.* RHE)	*j* (mA cm^{-2})	△*j* (mA cm^{-2})	FE-C_{2+} (%)	△FE-C_{2+} (%)	*Ref*
de-alloyed Cu-Al	1 M KOH	flow cell	-1.5	600	/	80	14	[1]
CeO_2 modified CuO	1 M KOH	flow cell	-1.12	1210	1191	75.2	26.9	[2]
$Cu_{0.80}Zn_{0.20}$ NPs	1 M KOH	flow cell	-0.53	200	/	30	25	[3]
F-Cu	0.75 M KOH	flow cell	-0.89	1600	/	80	/	[4]
Cu@NxC	0.1 M $KHCO_3$	H cell	-1.1	6.3	2.5	80	41	[5]

carbon/Cu/PTFE	0.5 M $KHCO_3$ + 0.5 M KCl (pH = 8.0)	flow cell	-0.89	500	/	82	10	[6]
Cu-12	1 M $KHCO_3$	flow cell	-0.83	322	-41	82.5	18	[7]
COF:PFSA-modified PTFE–Cu	phosphate solution with 3 M KCl (pH ≈ 1.0).	flow cell	/	250	0	78	78	[8]
polymer 8 modified Cu	0.1 M $KHCO_3$	flow cell	-1.04	4.7	-0.5	77.3	47.7	[9]
PTFTEB/Cu foil	0.1 M $KHCO_3$	H cell	-1.2	14.3	0.7	68.1	31.6	this work
PTFTEB-CuCl/ED-Cu	1 M KOH	flow cell	-1.2	304	7	56	18.5	

$\triangle j = j$ (modified Cu) - j (unmodified Cu)

$\triangle$FE-C_{2+} = FE-C_{2+} (modified Cu) - FE-C_{2+} (unmodified Cu)

S1. Definition of descriptors and metrics

1.1 LoFFi Features

The ECFP fingerprints do not accurately reflect the chemists' view of functional groups. To better add domain knowledge of functional groups, we defined Local Functional fingerprint (LoFFi).

First, LoFFi can automatically identify the aromatic rings and predefined functional groups in the molecule: the features of aromatic rings were generated when each new molecule was added, and small rings in fused rings are not recognized by the small ring features, such as benzene rings in naphthalene rings will not be independently documented. The aromatic feature list was appended if new type of aromatic ring

was detected. Second, the functional groups are formed by querying classic functional groups in real-time for each molecule.

Classic functional groups in LoFFi:

Alkene	1comma2-Diol	Carboxylic_ester	Oxoarene
Alkyne	1comma1-Diol	Lactone	Thioarene
Allene	Hydroperoxide	Carboxylic_anhydride	Nitrite
Alkylchloride	Peroxo	Thioacetate	Thionitrite
Alkylfluoride	Organometallic_compounds	Ethanethioic	Nitrate
Alkylbromide	Aldehyde	Amide	Nitro
Alkyliodide	Ketone	Lactam	Diazo
Alcohol	Thioaldehyde	Alpha_aminoacid	Azide
Dialkylether	Thioketone	Alpha_hydroxyacid	Hydrazine
Alkylarylether	Imine	Ketene	Hydrazone
Diarylether	Immonium	Nitrile	Sulfon
Diarylthioether	Oxime	Isonitrile	Sulfoxide
Oxonium	Oximether	Urea	Sulfuric_derivative
Primary_aliph_amine	Acetal	Thiourea	Sulfonic_derivative
Secondary_aliph_amine	Hemiacetal	Guanidine	Sulfinic_derivative
Tertiary_aliph_amine	Aminal	Isocyanate	Sulfenic_derivative
Quaternary_aliph_ammonium	Hemiaminal	Cyanate	Phosphine
Primary_arom_amine	Thioacetal	Isothiocyanate	Phosphine_oxide
Secondary_arom_amine	Thiohemiacetal	Thiocyanate	Phosphonium
Tertiary_arom_amine	Chloroalkene	Phenol	Phosphonic_acid_derivative
Quaternary_arom_ammonium	Fluoroalkene	1comma2-Diphenol	Phosphoric_acid_derivative
Ammonium	Bromoalkene	Arylchloride	Phosphinic_acid_derivative
Alkylthiol	Iodoalkene	Arylfluoride	Phosphonous_derivatives
Dialkylthioether	Enol	Arylbromide	Phosphinous_derivatives
Alkylarylthioether	Enamine	Aryliodide	Quart_silane
Disulfide	Acylhalide	Arylthiol	Non-quart_silane
1comma2-Aminoalcohol	Carboxylic_acid	Iminoarene	Silylmonohalide

1.2 LoFFi-MOE Features

There are two sections: LoFFi-MOE of the conjugated system and LoFFi-MOE of the full molecule. In conjugated system, only the longest conjugated sub-structure is considered and the features start with ‘Conju’, like 'Conju-Max-Distance'.

1.2.1 Brief definition of conjugation descriptors of LoFFi-MOE. For more details, see our previous work[10]

Feature	Brief definition
Num of Conju-Stru (MFF-Conju)	The number of conjugation structures
Num of Conju-All-Atoms (MFF-Conju)	The number of atoms in conjugation structures
Atom Num Conju-All Ratio (MFF-Conju)	The number of atoms in all conjugation structures divided by the number of atoms
AtomWt Conju-All Ratio (MFF-Conju)	The sum of weight of all conjugation structures divided by the molecular weight.
Full-Mol Wiener Index (MFF-Conju)	Wiener Index of the whole molecule.
Individual Conju-Atom Number (MFF-Conju)	The number of atoms in the longest conjugated structure in one molecule.
Conju-Part-Wt (MFF-Conju)	The maximum weight of all conjugation structures in one molecule.
Conju-AtomicWt (MFF-Conju)	The maximum atomically averaged weight of all conjugation structures in one molecule.
Max Conju-Distance (MFF-Conju)	The maximum conjugated length
Conju-Branch Index (MFF-Conju)	The maximum branching index in conjugated part of molecule
Conju-Stru Wiener Index (MFF-Conju)	Wiener Index of the conjugated part of one molecule.
Conju-Stru-VSA (MFF-Conju)	The approximate surface area of all conjugation structures in one molecule.
Max Distance	The maximum length in whole molecule
Branch Index	The maximum branching index in whole molecule
Stru-VSA	The approximate surface area in whole molecule

The rest of LoFFi-MOE descriptors could be calculated in our featurization algorithm (LoFFi-MOE): 'PEOE-Charge', 'LogP', 'MR'. The value of the properties is obtained by the summation of values of its containing atoms.

Taking “PEOE Charge” as an example, we sum up the Gasteiger atomic charges of atoms in a LoFFi fragment. The maximum and minimum of these summed PEOE charges of all fragments were then extracted as two molecular features: “PEOE-Charge-Max” and “PEOE-Charge-Min”.

LogP is the logarithm of oil (octanol)–water partition coefficient of a molecule. The atomic attribution of LogP effectively explores the local polarity of a molecule. The summation of atomic LogP to LoFFi can identify polar groups in the molecule. Similarly, the MR is the polarizability of the molecule determined by molar refractivity. The atomic attribution of the MR highlights the polarizability of each atom in a molecule, while its summation to the LoFFi shows the polarizability of a conjugated fragment.

The atomic PEOE charge, contribution of LogP, and contribution of MR are calculated by the RDKit toolkit.

The following features have 'Px' in the names. The 'Px' stands for names of different properties as shown in the table below.

P_x	property
x=1	PEOE-Charge
x=2	LogP
x=3	MR

'P_(x,i,k)' means the xth atomic property of the kth atom in the ith molecule.

1.2.2.1 'P_x -Sum'

The sum of atomic properties of atoms in the conjugation structure. If multiple conjugation structures are present in one molecule, then the value of the one with the maximum number of atoms will be used (similarly hereinafter).

$$F_{x,i} = \sum_{k}^{N_{atoms,i,j}} P_{x,i,j,k}$$

1.2.2.2 'P_x-AtomicMean

The atomic averaged value of atomic properties of atoms in the conjugation structure.

$$F_{x,i} = \frac{1}{N_{atoms,i,j}} \sum_{k}^{N_{atoms,i,j}} P_{x,i,j,k}$$

1.2.2.3 'P_x-Maximum'

The maximum value of properties of single atoms and all possible MFF fragments in the conjugation structure. The sum of atomic properties in a MFF fragment is calculated first as fragment property. Then the maximum value is picked out from all the single atom properties together with all fragment properties.

$$P_{x,i,j,m} = \sum_{k}^{N_{atoms,i,j,m}} P_{x,i,j,k}$$

The fragment properties will be noted as '$P_{x,i,j,m}$' which means the property of the m^{th} fragment in the j^{th} conjugation structure of the i^{th} molecule. $N_{atoms,i,m}$ represents the atom index of the m^{th} fragment in the j^{th} conjugation structure of the i^{th} molecule.

$$F_{x,i} = \max\left(P_{x,i,j,k}(k = 1, 2, \dots, N_{atoms,i,j}), P_{x,i,j,m}\ (m = 1, 2, \dots, N_{frags,i,j})\right)$$

$N_{frags,i,j}$ means the number of fragments in the j^{th} conjugation structure of the i^{th} molecule.

1.2.2.4 'P_x-Minimum'

The minimum value of properties of single atoms and all possible MFF fragments in the conjugation structure.

$$F_{x,i} = \min\left(P_{x,i,j,k}(k = 1, 2, \dots, N_{atoms,i,j}), P_{x,i,j,m}\ (m = 1, 2, \dots, N_{frags,i,j})\right)$$

1.2.2.5 'P_x-Delta'

The difference between the maximum and minimum properties of single atoms and all possible MFF fragments in the conjugation structure.

$$F_{x,i} = \max\left(P_{x,i,j,k}(k = 1, 2, \dots, N_{atoms,i,j}), P_{x,i,j,m}\ (m = 1, 2, \dots, N_{frags,i,j})\right) - \min\left(P_{x,i,j,k}(k = 1, 2, \dots, N_{atoms,i,j}), P_{x,i,j,m}\ (m = 1, 2, \dots, N_{frags,i,j})\right)$$

1.2.2.6 'P_x-STD

The standard deviation of atomic properties of atoms in the conjugation structure.

$$F_{x,i} = \sqrt{\frac{1}{N_{atoms,i,j}} \sum_{k}^{N_{atoms,i,j}} (P_{x,i,j,k} - \mathbf{Px} - \mathbf{AtomicMean})}$$

1.2.2.7 'P_x-MaxMinDisRatio'

The ratio between the distance of the single atoms or fragments with the maximum property and the minimum property over the maximum distance of conjugation structure.

$$F_i = \frac{\max\{d_{i,j,p',q'}\}}{\max\{d_{i,j,p,q}\}}$$

p', q' is the atomic index of the single atom or the fragment with maximum and minimum properties. $d_{i,j,p',q'}$ stands for the longest distance of two atoms in the fragments with maximum and minimum properties.

1.2.2.8 'P_x-CONJUMAX'

The sum of atomic properties of atoms in the conjugation structure. If multiple conjugation structures are present in one molecule, then all of the value of every conjugated atoms will be used.

$$F_{x,i} = \sum_{k}^{N_{atoms,i}} P_{x,i,j,k}$$

1.2.3 Brief definition about LoFFi-MOE of the whole molecule.

In case the conjugation condition is not important, the variation j^{th} conjugation structure is ignored. When a descriptor entitled with "Atomic", it represents the consideration of the whole molecule. When entitled with "Conju", only the conjugated part is considered.

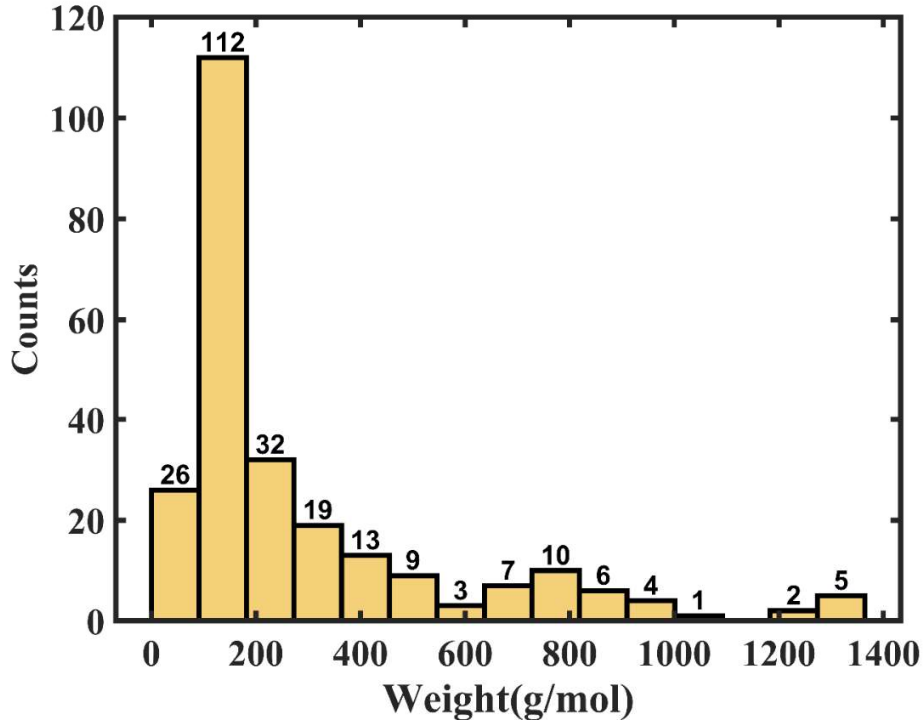

Figure S1. Molecular weight distribution of organic modifiers in the 237 samples.

1.3 Experiment condition and polymerization parameter

Typical voltage (V vs RHE): Standard voltage measurement referenced against the reversible hydrogen electrode (RHE).

Typical current density (mA/cm²): Average electrical current passing through a unit area of the electrode surface during electrolysis.

Delta_current density ratio: Ratio of the change in current density to the initial current density of bare Cu.

Is_Voltage_reliable: Indicates whether the voltage measurement is considered reliable (true or false).

Is_current_density_reliable: Indicates whether the current density measurement is considered reliable (true or false).

Typical pH: Average or representative pH value of the electrolyte solution, including neutral and weak base.

Typical electrolyte: Description of the electrolyte solution used in the experiment.

Is_constant_current: Indicates whether a constant current was applied during the experiment (true or false).

Cell type: Describes the type of electrochemical cell used, including H-cell, GDE and MEA.

Is_Polymerized: Indicates whether a polymerized material was used or involved in the experiment (true or false).

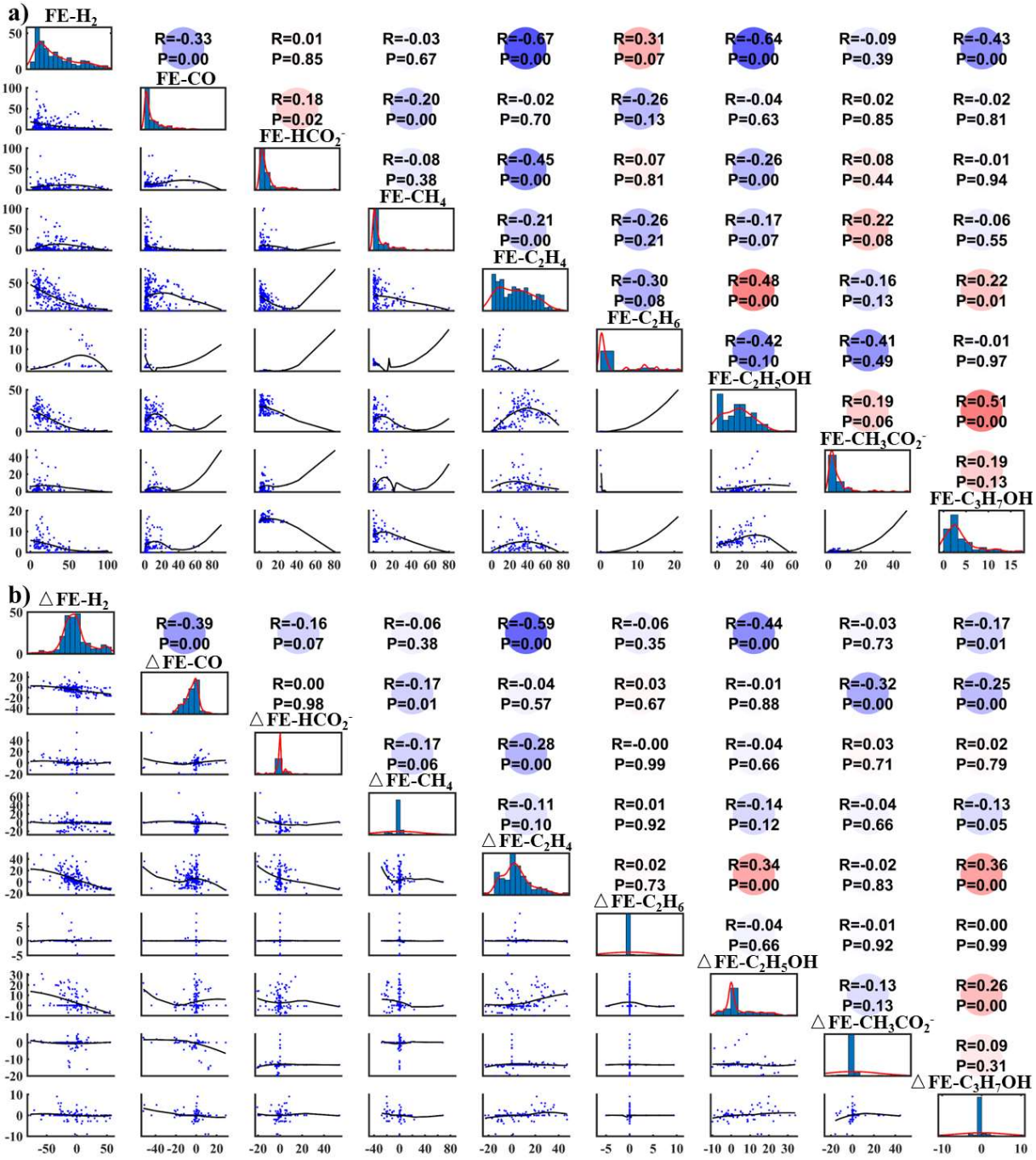

Figure S2. Pair plot of correlation between the a) ΔFEs and b) FE of different products. The R values are Pearson correlation coefficients, while the p values are from the hypothesis test using the Pearson correlation.

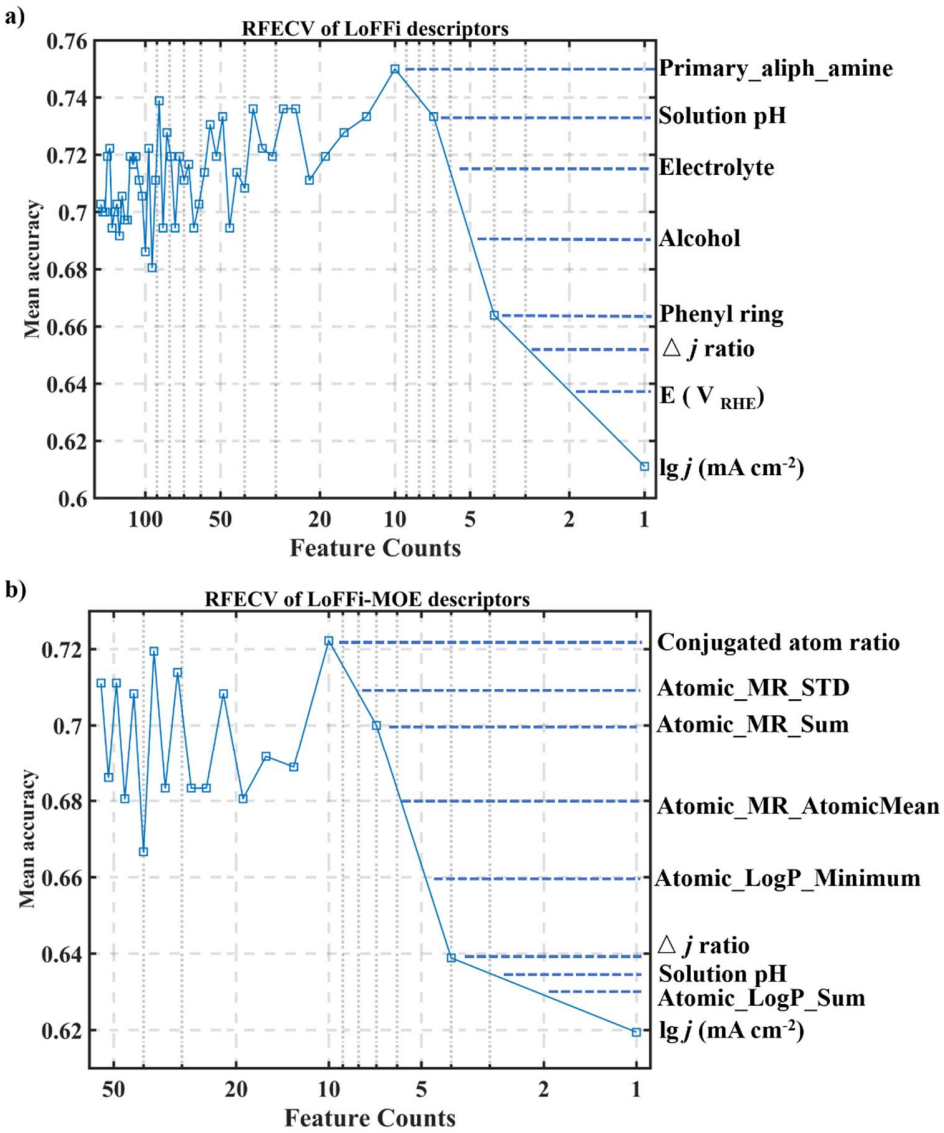

Figure S3. Procedure of RFECV in machine learning using a) LoFFi and b) LoFFi-MOE descriptors. Selected descriptors were shown on the right side of the figure and sorted by Permutation importance of GBCT.

S2. Model performance and SHAP analysis of LoFFi descriptors

Table S2. Classification performance based on LoFFi 237×149 feature matrix.

Feature Type	Feature size	Model	roc_auc_score	Accuracy	f1 score
LoFFi	149	Decision Tree	0.539	0.547	0.441
		GBCT	0.803	0.758	0.706
		Logistic Regression	0.721	0.667	0.608
		MLP	0.614	0.528	0.36
		k-Nearest Neighboirs	0.778	0.722	0.696
		Random forest	0.726	0.700	0.592
		SVC	0.728	0.694	0.619
		XGB	0.795	0.758	0.720

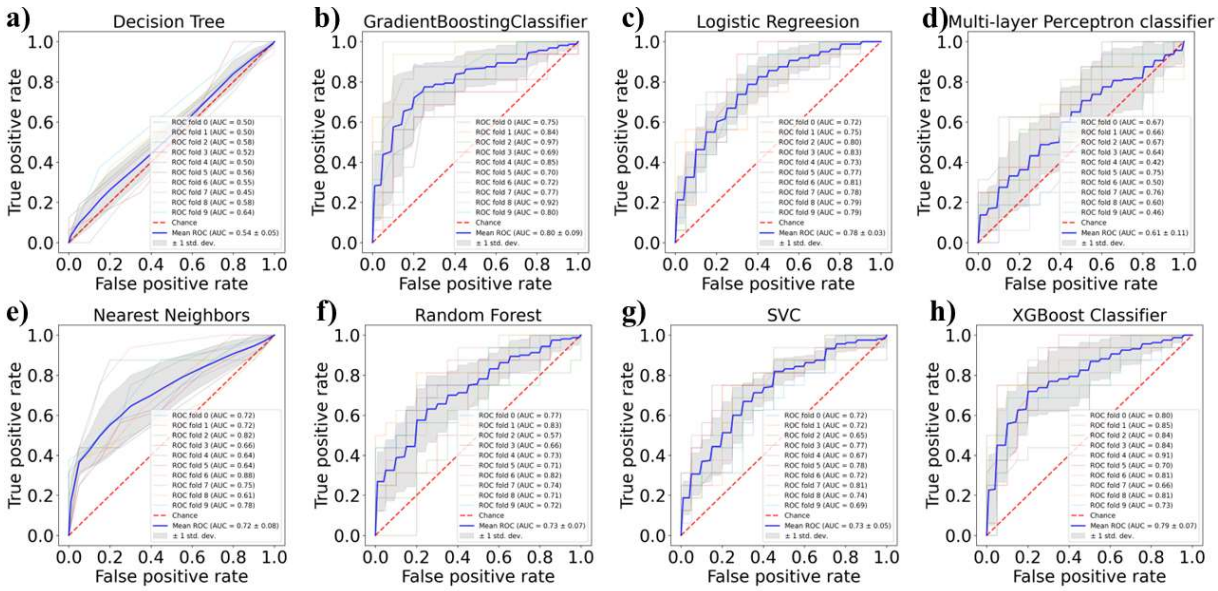

Figure S4. ROC response of 8 models based on LoFFi/ condition / polymerization descriptors, created from 10-fold cross-validation.

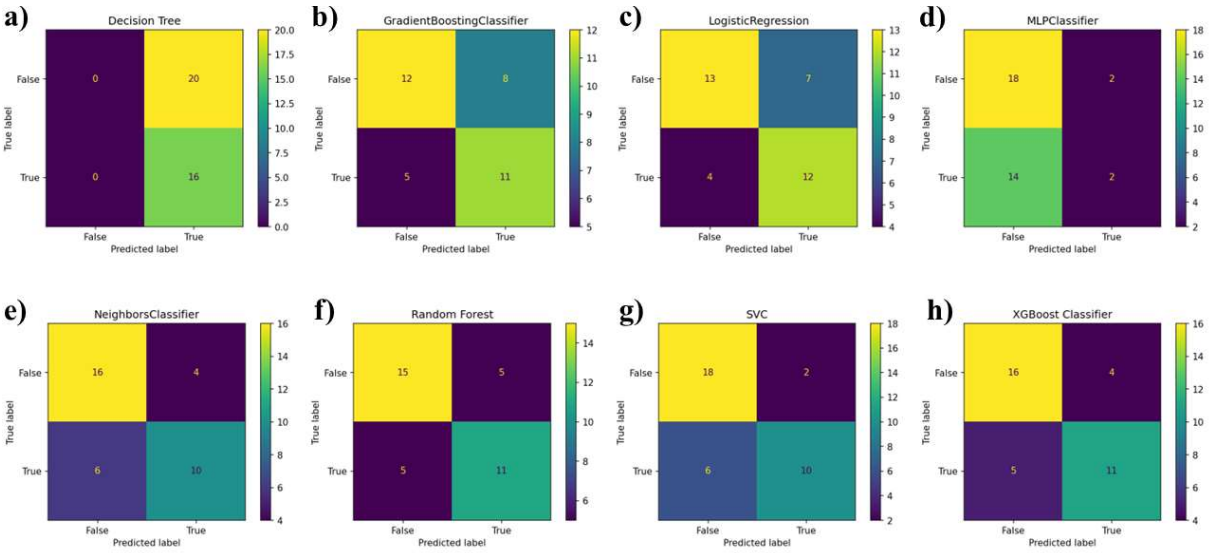

Figure S5. Confusion matrix of 8 models based on LoFFi / condition / polymerization descriptors.

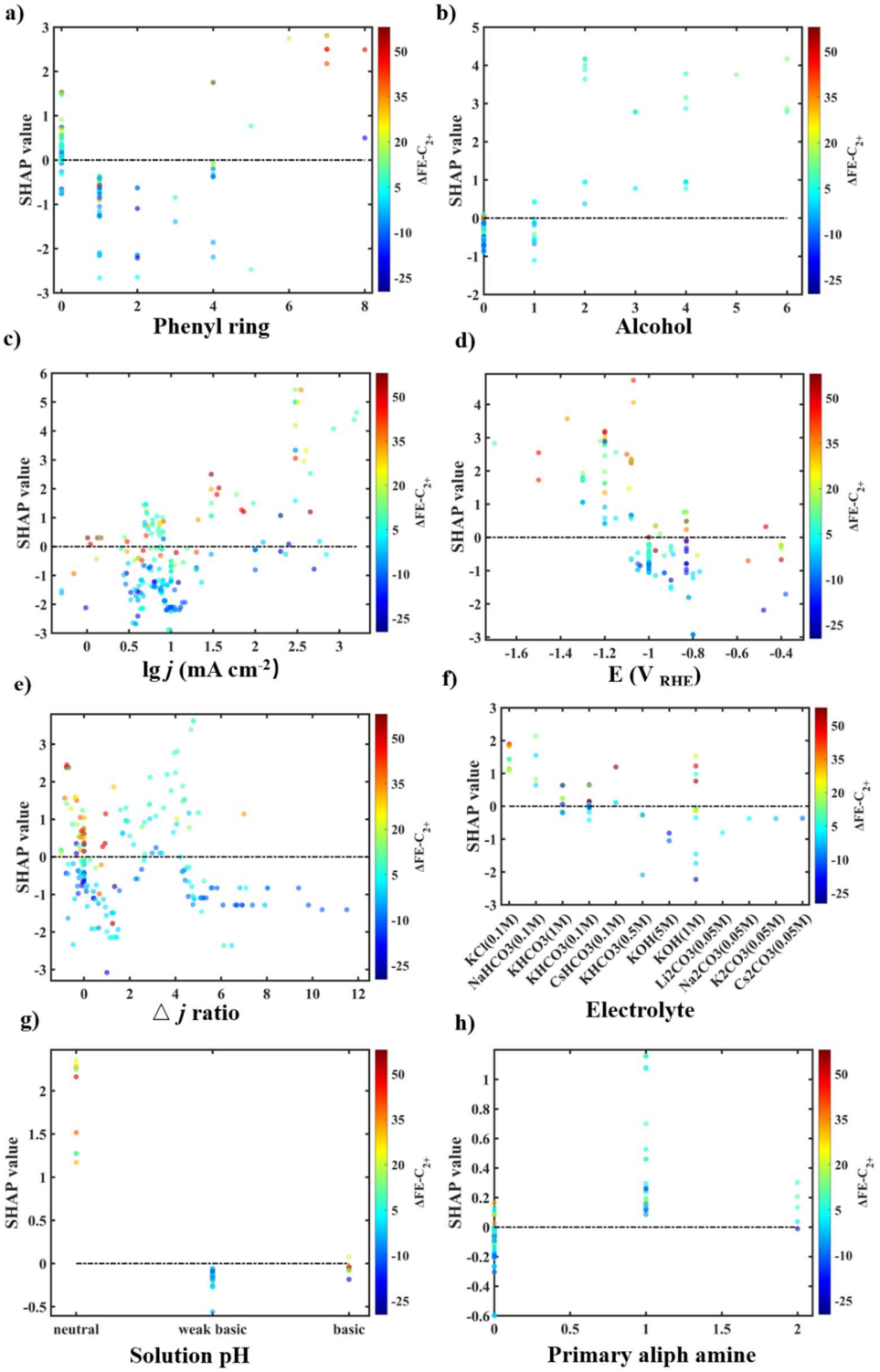

Figure S6. SHAP analysis of GBCT based on LoFFi/ condition / polymerization descriptors. The color bar denotes $\Delta FE\text{-}C_{2+}$. Black dash line helps to recognized the mean contribution. Scatter points below the black dash line correspond negative effect, and vice versa.

S3. Model performance and SHAP analysis of LoFFi-MOE descriptors

Table S3. Classification performance from 10-fold cross-validation based on LoFFi-MOE 222×54 feature matrix.

Feature Type	Feature size	Model	roc_auc_score	Accuracy	f1 score
LoFFi-MOE	54	Decision Tree	0.683	0.600	0.559
		GBCT	0.853	0.733	0.688
		Logistic Regression	0.707	0.672	0.668
		MLP	0.726	0.686	0.655
		k-Nearest Neighboirs	0.630	0.594	0.574
		Random forest	0.799	0.750	0.705
		SVC	0.751	0.669	0.602
		XGB	0.777	0.728	0.692

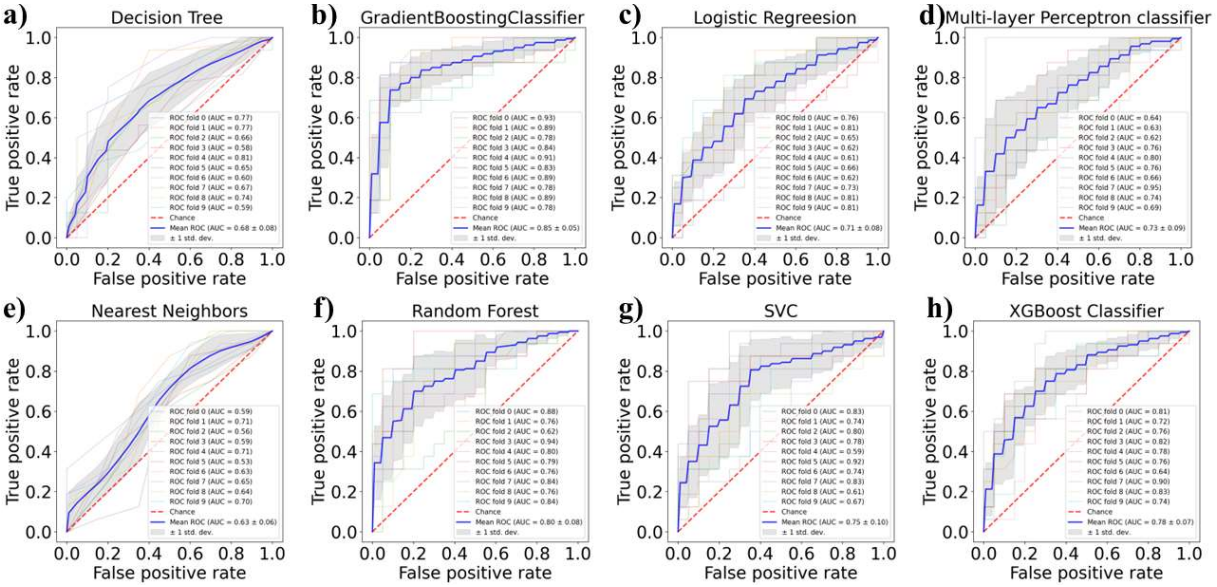

Figure S7. ROC response of 8 models based on LoFFi-MOE/ condition / polymerization descriptors, created from 10-fold cross-validation.

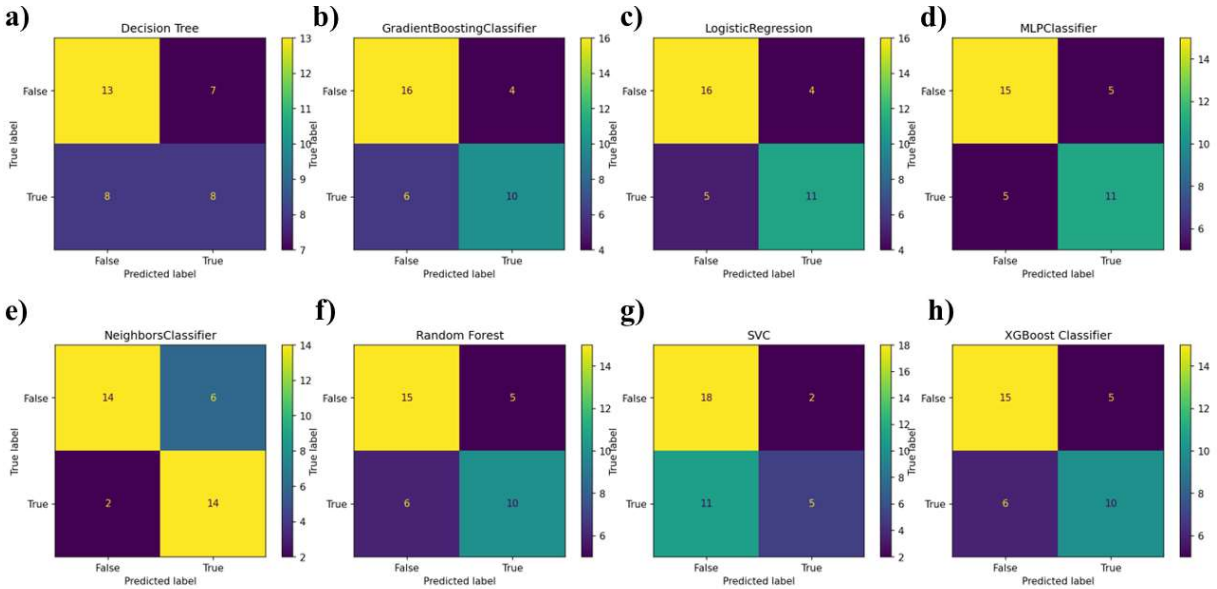

Figure S8. Confusion matrix of 8 model based on LoFFi-MOE/ condition / polymerization descriptors.

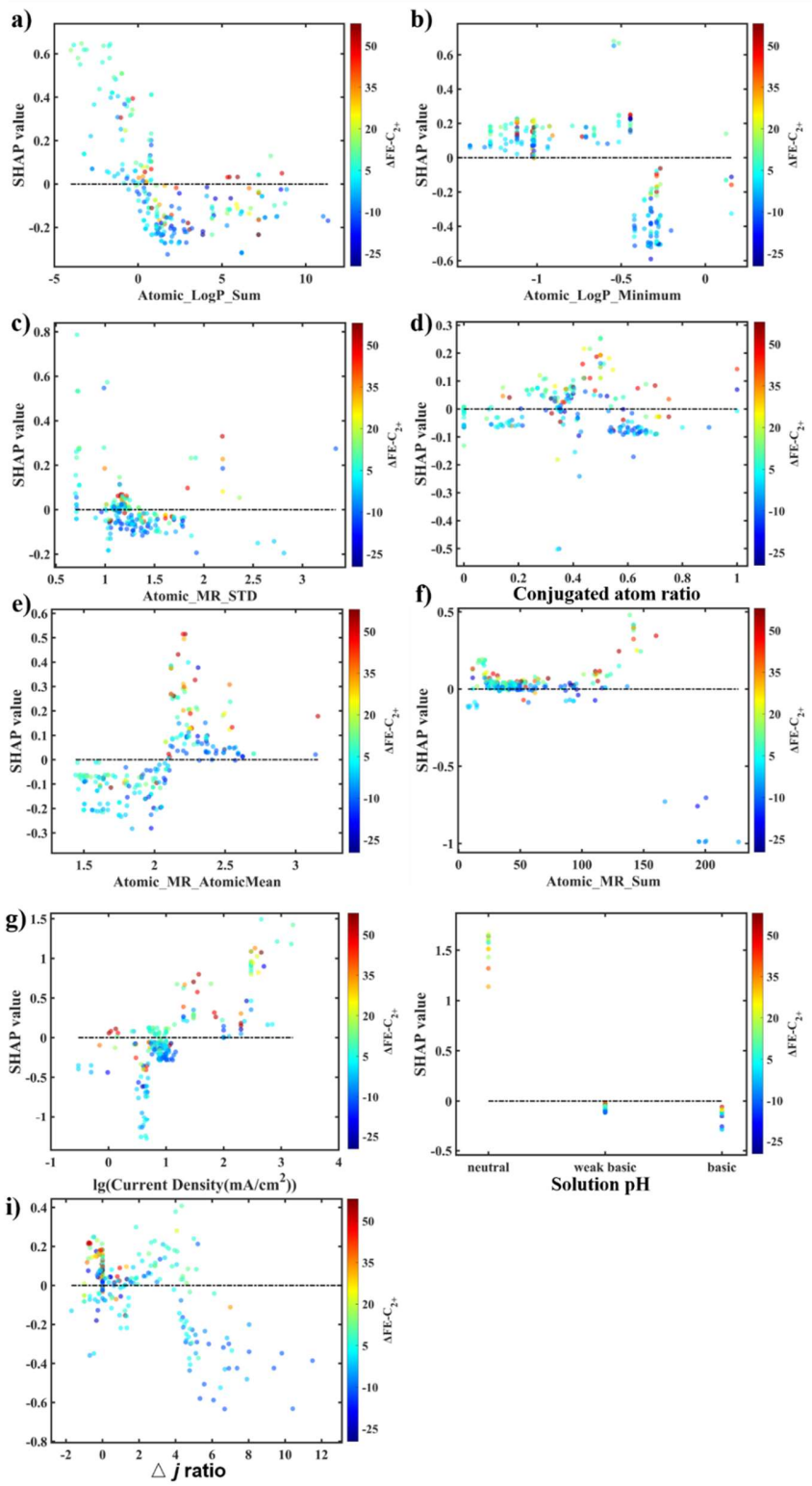

Figure S9. SHAP analysis of GBCT based on LoFFi-MOE/ condition / polymerization descriptors. The color bar denotes ΔFE-C_{2+}. Black dash line helps to recognize the mean contribution. Scatter points below the black dash line correspond negative effect, and vice versa.

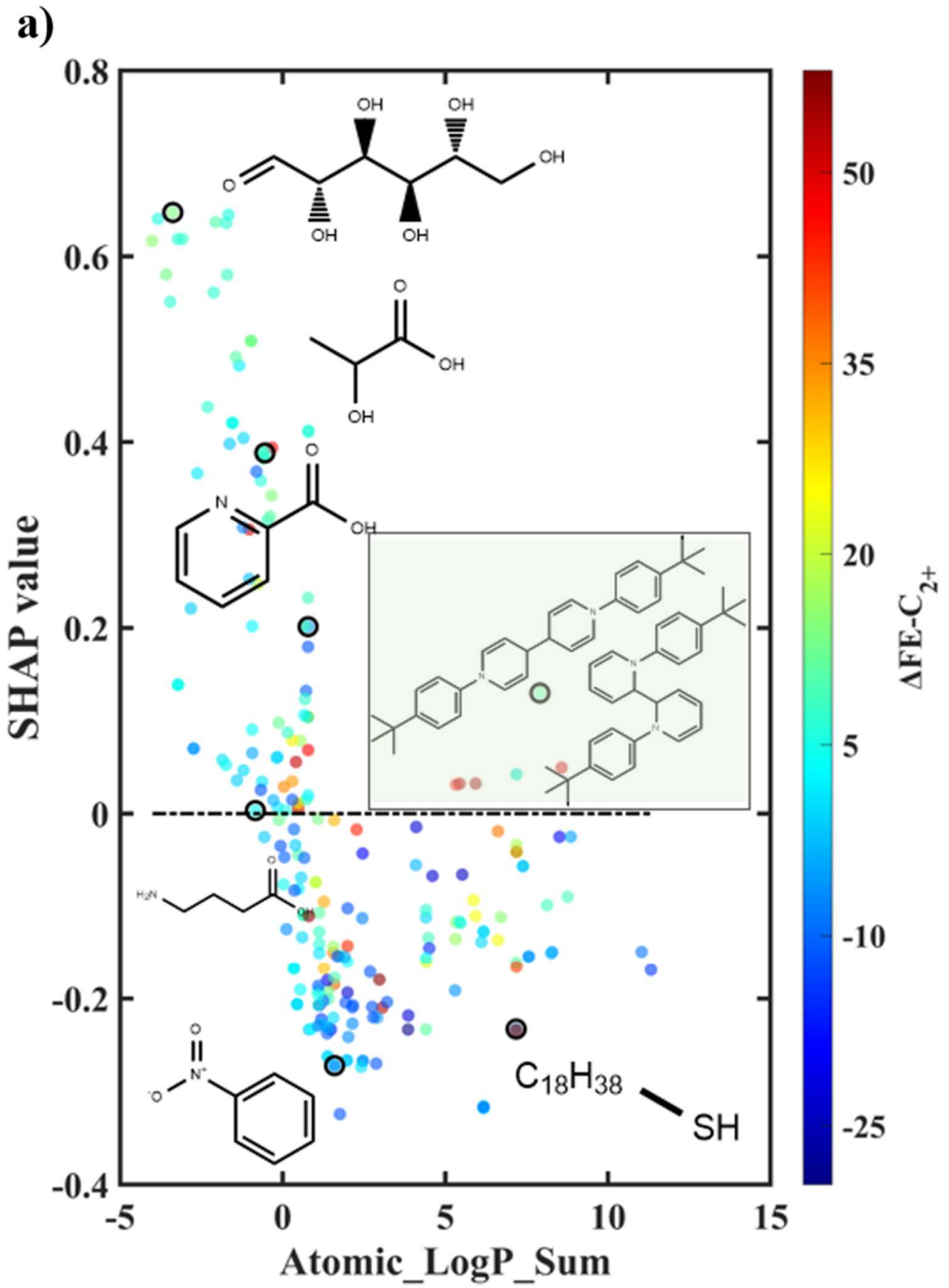
a)
SHAP value
Atomic_LogP_Sum
ΔFE-C2+
C18H38
SH

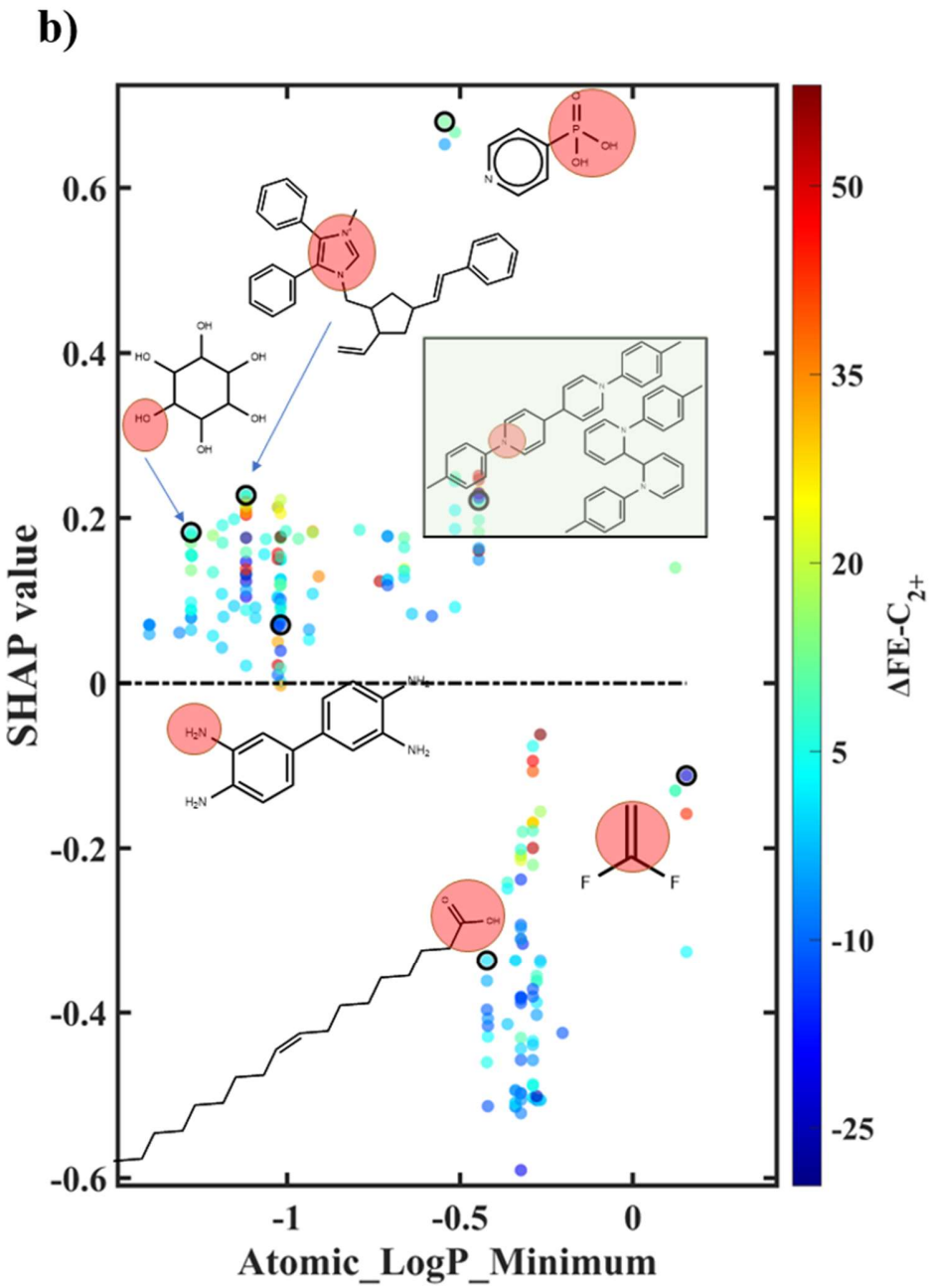
b)
SHAP value
0.6
0.4
0.2
0
-0.2
-0.4
-0.6
-1
-0.5
0
Atomic_LogP_Minimum
50
35
20
5
-10
-25
ΔFE-C2+
OH
HO
NH2
F
O
P

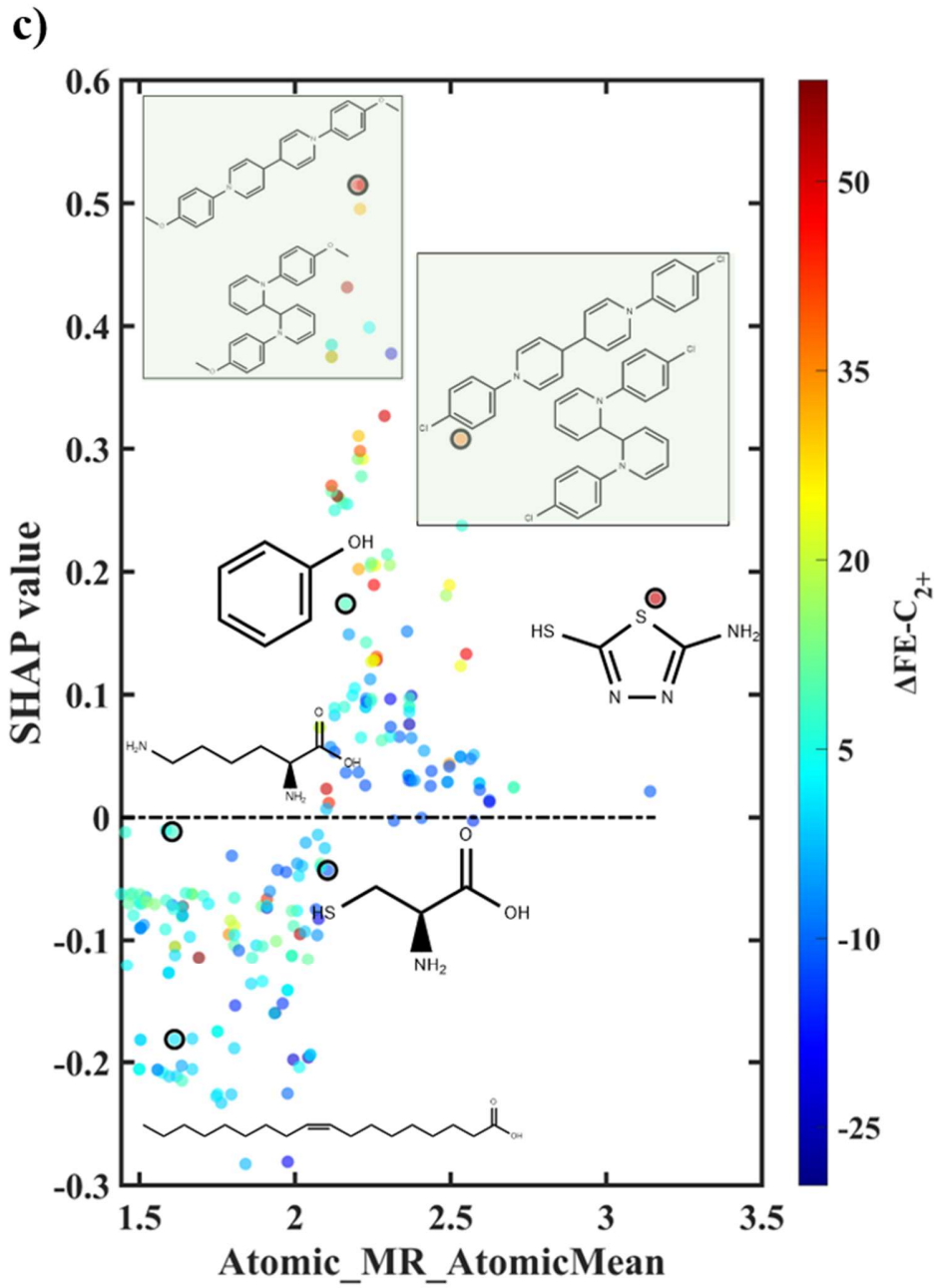

Figure S10. SHAP plots with molecules examples, a) Atomic_LogP_Sum, b) Atomic_LogP_Minimum and c) Atomic_MR_AtomicMean. The black circled scatter point highlighted some examples, with molecular structure nearby. The color of each scatter point refers to C_{2+}-FE differences indicated by the right colorbar. The pink shadow in **Figure S10b** highlights the functional group which has minimum LogP value in the molecule.

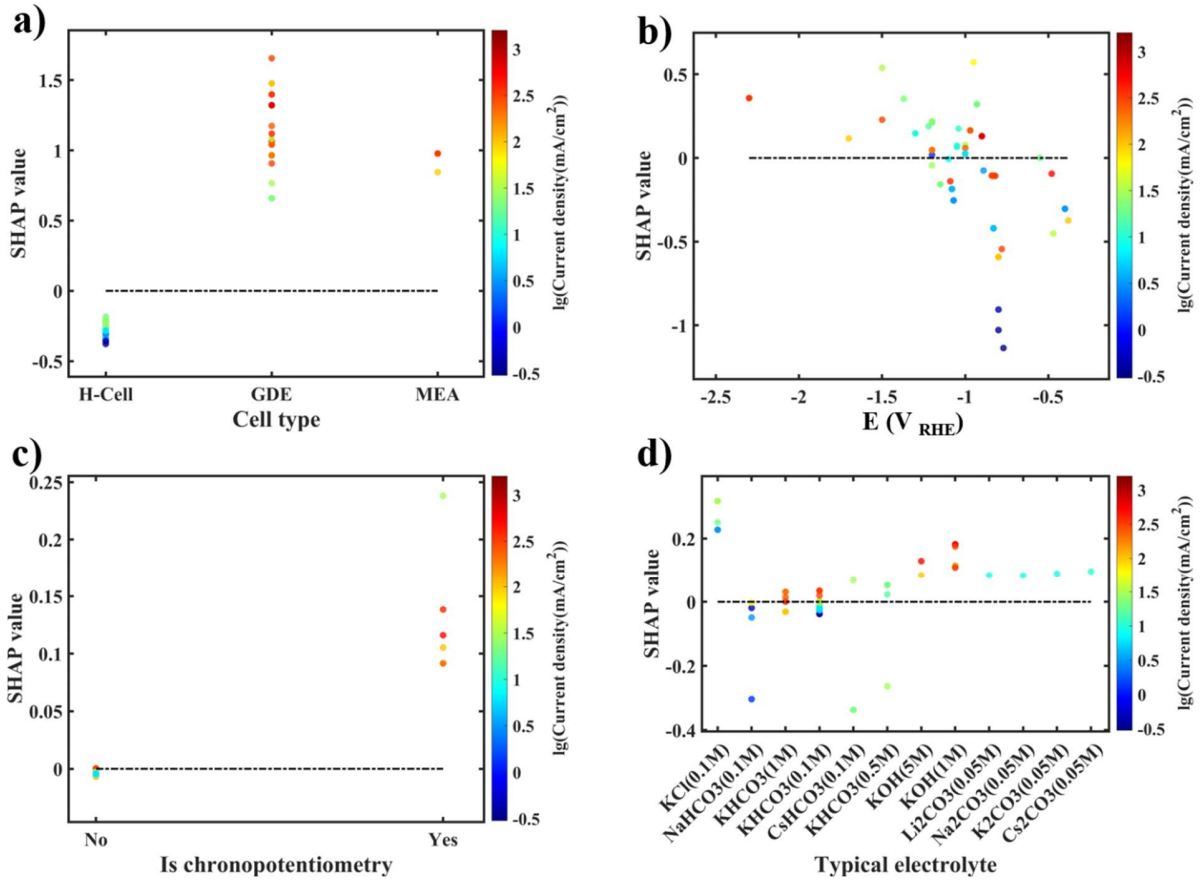

Figure S11. SHAP analysis in the machine learning of the current density using XGBoost model.

S4. Synthesis and Characterization of monomers

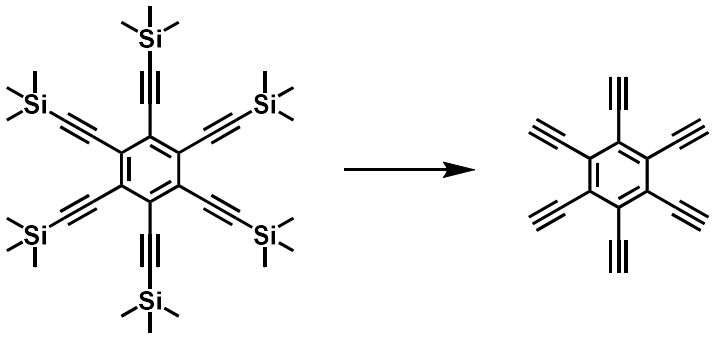

HEB-TMS HEB

(1) HEB[11]: 9 mg of 1,2,3,4,5,6-hexa((trimethylsilyl)ethynyl)benzene was dissolved in 8 mL of THF with stirring at 0 °C under an argon atmosphere. After the addition of 1 mL of TBAF (1M THF), the reaction was held at 0 °C for 20 min. The solution was diluted with dichloromethane (10 mL) and washed three times with saturated brine (10 mL), dried over anhydrous magnesium sulfate to remove the solid, and distilled under reduced pressure to obtain 1,2,3,4,5,6-hexanol acetylene benzene. The monomer is not stable, and it is used by hydrolysis.

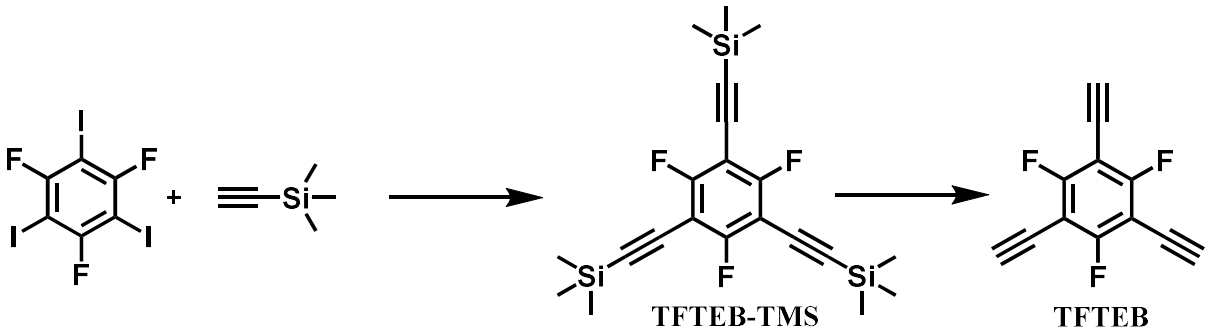

TFTEB-TMS TFTEB

(2) TFTEB[12]: Under N_2 atmosphere, 1,3,5-trifluoro-2,4,6-triiodobenzene (500 mg, 0.98 mmol), $PdCl_2(PPh_3)_2$ (21 mg, 3 mol- %), CuI (6 mg, 3 mol-%), PPh_3 (20 mg, 3 mol-%) and DIPA (27 mL) were added to a dry three-necked flask. To the reaction solution was added ethynyltrimethylsilane (2.1 mL, 13.7 mmol) dropwise with a syringe from a branch port. At the end of the addition, the mixture was warmed to 80°C. After 1 hour, THF (9 mL) was added and the mixture was stirred under nitrogen for 16 hours. The mixture was filtered through celite, the filtrate was collected. The solvent evaporated to give a solid. It was dissolved in chloroform and extracted with saturated brine, washed three times, and the organic phase was collected by separation and dried with anhydrous Na_2SO_4. After the solvent was evaporated, the obtained brownish-yellow solid was purified by silica gel chromatography (hexane as eluent) to obtain 1,3,5-(trimethylsilyl)ethynyl 2,4,6-Trifluorobenzene [white powder, 85% yield]. ^1H NMR (500 MHz, $CDCl_3$) δ 0.26 (s, 27H). 6 mg of 1,3,5-(trimethylsilyl)ethynyl 2,4,6-trifluorobenzene was dissolved in 8 mL of THF at 0°C under stirring in argon atmosphere. After the addition of 1 mL of TBAF (1M THF), the reaction was kept at 0 °C for 20 min. The solution was diluted with dichloromethane (10 mL) and washed three times with saturated brine (10 mL), dried with anhydrous Na_2SO_4. After the solvent was evaporated, obtain 1,3,5-triethynyl-2,4,6-trifluorobenzene. Monomer hydrolysis is now used.

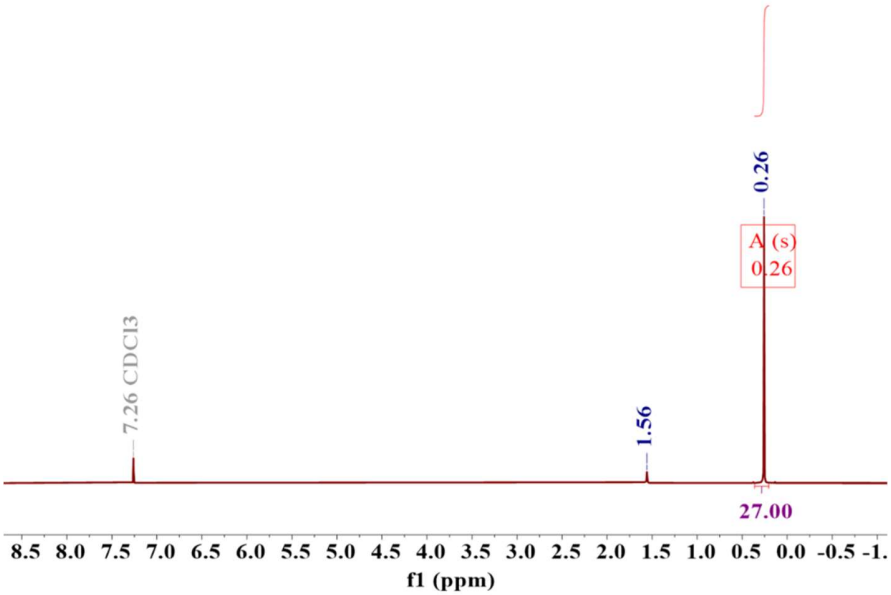

Figure S12. ^{1}H NMR of TFTEB-TMS in $CDCl_3$ at R.T.

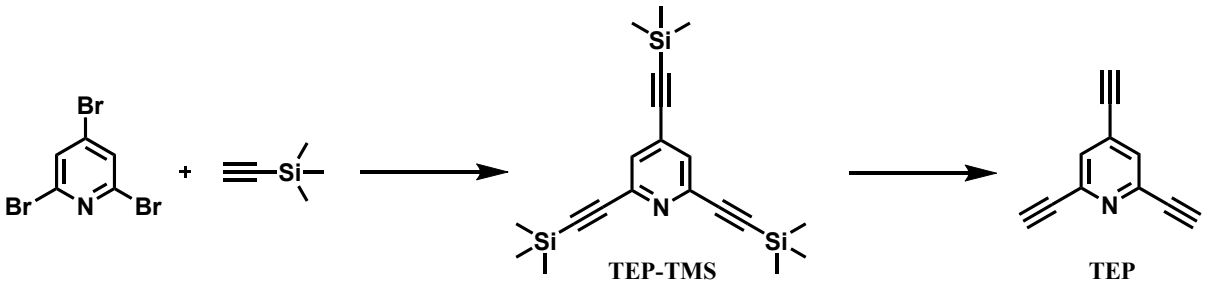

(3) TEP[13]: Under N_2 atmosphere, 2,4,6-tribromopyridine (190 mg, 0.6 mmol), $PdCl_2(PPh_3)_2$ (21 mg, 5 mol-%) CuI (6 mg, 5 mol-%), DIPA (2 mL) and dioxane (8 mL) were added to a dry three-necked flask, and ethynyltrimethylsilane (1.3 mL, 9 mmol) was added dropwise to the reaction solution using a syringe from the branch port of the reaction flask. At the end of the addition, the reaction was warmed to 80°C and stirred for one day. The black precipitate formed by the reaction was removed by diatomaceous earth suction filtration, the organic filtrate was collected, and the solvent was evaporated. The dichloromethane dissolved product was extracted with saturated brine, washed three times. The organic phase was collected and dried with anhydrous Na_2SO_4. The organic solvent was removed and purified by silica gel chromatography with hexane as the eluent to obtain 2,4,6-tris((trimethylsilyl)ethynyl)pyridine [brownish yellow crystals, 70% yield]. ^{1}H NMR (500 MHz, $CDCl_3$) δ 7.41 (d, J = 1.4 Hz, 2H), 0.24 (d, J = 1.5 Hz, 28H). 5 mg of 2,4,6-tris((trimethylsilyl)ethynyl)pyridine was dissolved in 8 mL of THF with stirring at 0 °C under argon atmosphere. After the addition of 1 mL of TBAF (1 M THF), the reaction was kept at 0 °C for 20 min. The solution was diluted with dichloromethane (10 mL) and washed three times with saturated brine (10 mL), dried with anhydrous Na_2SO_4. After the solvent was evaporated, obtain 2,4,6-triethynylpyridine. Monomer hydrolysis is now used.

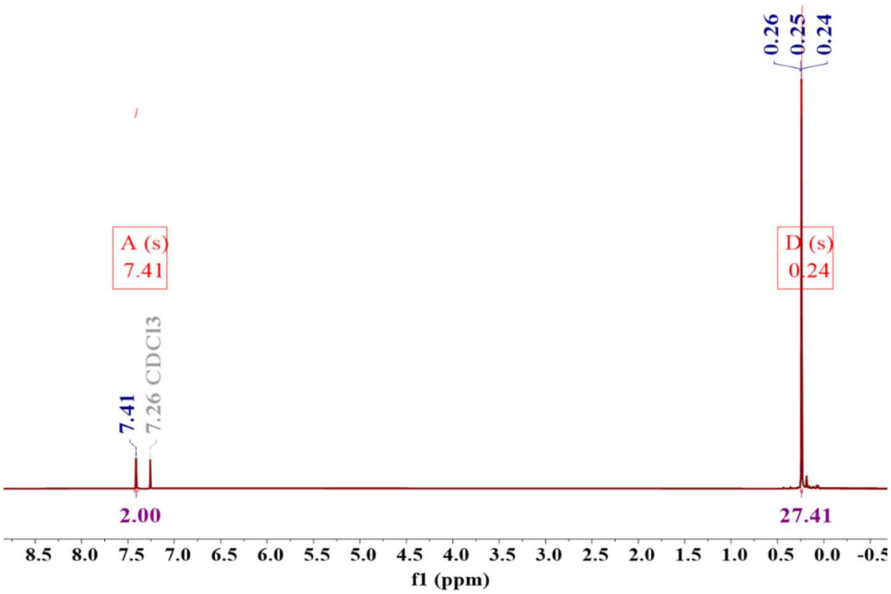

Figure S13. ^{1}H NMR of TEP-TMS in $CDCl_3$ at R.T.

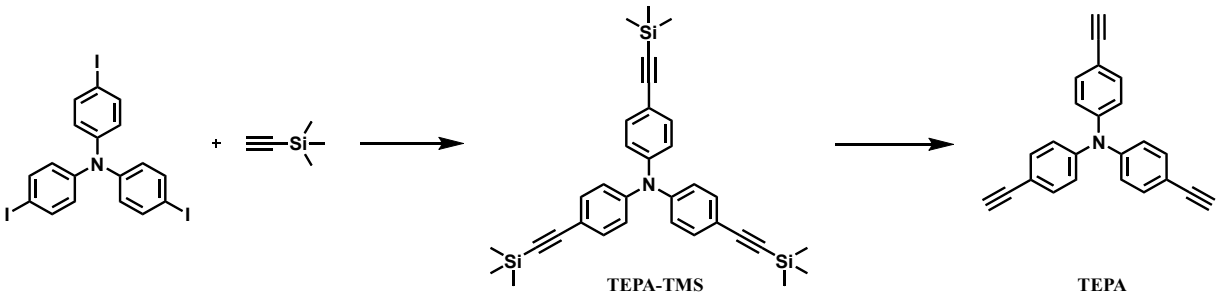

(4) TEPA[14]: Under N_2 atmosphere, tris(4-iodophenyl)amine (374 mg, 0.6 mmol), $PdCl_2(PPh_3)_2$ (21 mg, 5 mol-%), CuI (6 mg, 5 mol-%) DIPA (2 mL) and dioxane (8 mL) were added to a dry three-necked flask. To the reaction solution was added ethynyltrimethylsilane (1.3 mL, 9 mmol) dropwise with a syringe from a branch port. At the end of the addition, the mixture was warmed to 80 °C and stirred under nitrogen for one day. The mixture was filtered through celite to remove the black precipitate, the filtrate was collected, and the solvent was evaporated. It was dissolved in chloroform and extracted with saturated brine, washed three times, and the organic phase was collected by separation and dried with anhydrous Na_2SO_4. The organic solvent was removed and purified by silica gel chromatography with hexane as the eluent to obtain tris(4-((trimethylsilyl)ethynyl)phenyl)amine [yellow powder, 78% yield]. ^{1}H NMR (500MHz, $CDCl_3$) δ 7.34 (d, J = 8.7 Hz, 6H), 6.95 (d, J = 8.8 Hz, 6H), 0.24 (s, 27H). 7 mg of tris(4-((trimethylsilyl)ethynyl)phenyl)amine was dissolved in 8 mL of THF with stirring at 0 °C under argon atmosphere. After the addition of 1 mL of TBAF (1 M THF), the reaction was kept for 20 min. The solution was diluted with dichloromethane (10 mL), washed three times with saturated brine (10 mL), dried over anhydrous magnesium sulfate to remove solids, and distilled under reduced pressure to obtain tris(4-(ethynyl)phenyl)amine. Monomer hydrolysis is now used.

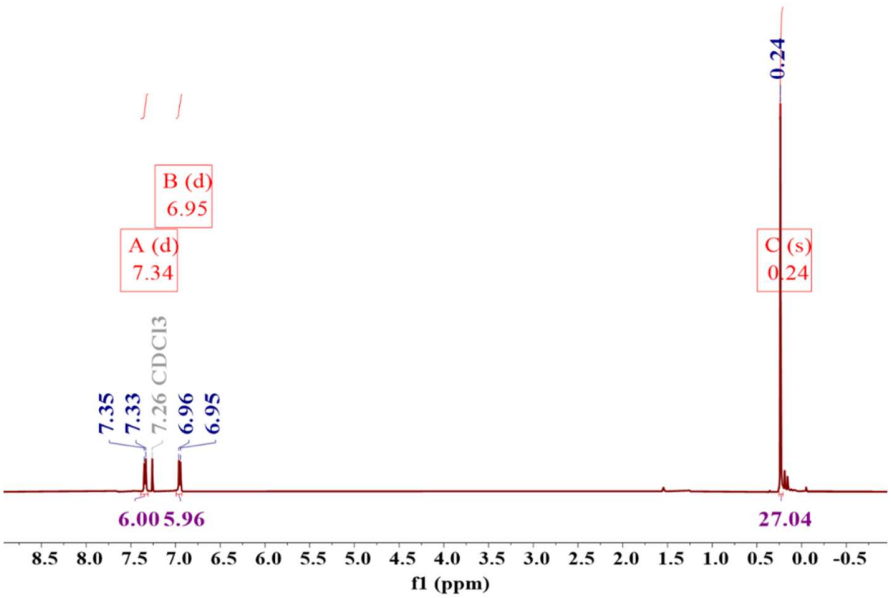

Figure S14. ^{1}H NMR of TEPA-TMS in $CDCl_3$ at R.T.

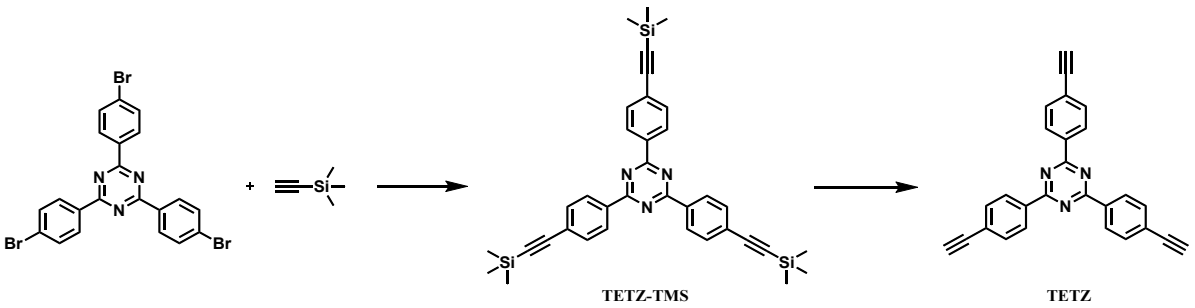

(5) TETZ[15]: Under nitrogen atmosphere, 2,4,6-Tris(4-bromophenyl)-1,3,5-triazine (328 mg, 0.6 mmol), $PdCl_2(PPh_3)_2$ (21 mg, 5 mol-%), CuI (6 mg, 5 mol-%), DIPA (2 mL), and dioxane (8 mL) were added to a dry three-necked flask. To the reaction solution was added ethynyltrimethylsilane (1.3 mL, 9 mmol) dropwise with a syringe from a branch port. At the end of the addition, the mixture was warmed to 60°C and stirred under nitrogen for two days. The mixture was filtered through celite to remove the black precipitate, the filtrate was collected and the solvent was evaporated. It was dissolved in chloroform and extracted with saturated brine, washed three times, and the organic phase was collected by separation and dried with anhydrous Na_2SO_4. The organic solvent was evaporated and the resulting yellow solid was purified by silica gel chromatography (hexane as eluent) to give 2,4,6-tris(4-((trimethylsilyl)ethynyl)phenyl) -1,3,5-triazine [white powder, 81% yield] . ^{1}H NMR (500 MHz, $CDCl_3$) δ 8.69 (d, J = 8.4 Hz, 6H), 7.65 (d, J = 8.4 Hz, 6H), 0.30 (s, 27H). 8 mg of 2,4,6-tris(4-((trimethylsilyl)ethynyl)phenyl)-1,3,5-triazine was dissolved in 8 mL with stirring at 0 °C under argon atmosphere in THF. After the addition of 1 mL of TBAF (1 M THF), the reaction was held at 0 °C for 20 min. The solution was diluted with dichloromethane (10 mL) and washed three times with saturated brine (10 mL), dried over anhydrous magnesium sulfate to remove the solid, and the solvent was evaporated to obtain 2,4,6-tris(4-ethynylphenyl))-1,3,5-triazine. Monomer hydrolysis is now used.

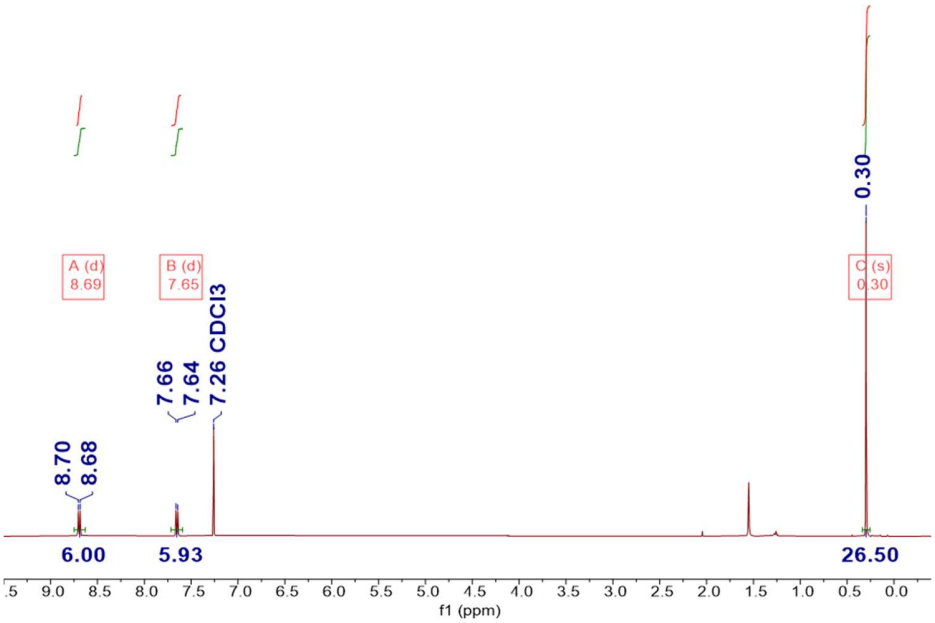

Figure S15. ^{1}H NMR of TETZ-TMS in $CDCl_3$ at R.T.

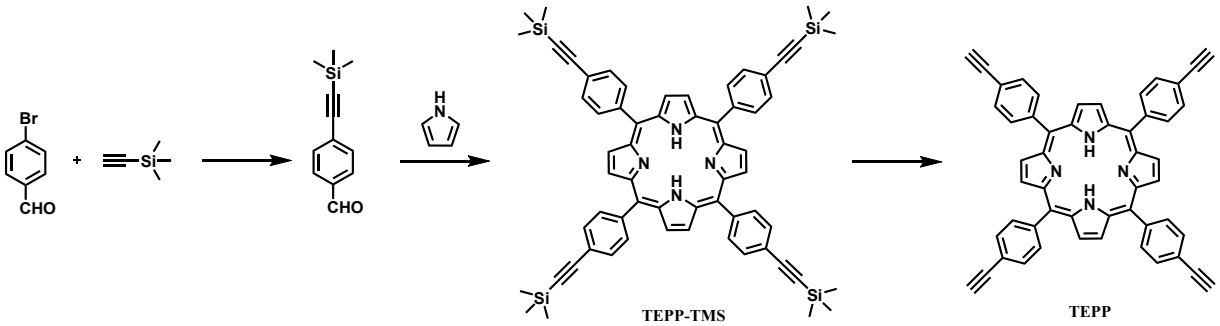

(6) TEPP[16]: Under nitrogen atmosphere, p-bromobenzaldehyde (5 g, 27 mmol), $PdCl_2(PPh_3)_2$ (382 mg, 0.54 mmol), CuI (206 mg, 1.08 mmol), THF/Et_3N=4:1 (v/v) 62.5 mL of mixed solvent was added to a 250 mL two-necked flask. Trimethylethynylsilicon (5 mL, 35 mmol) was slowly added dropwise to the system from the mouth of the flask with a syringe, and the reaction was stirred overnight at room temperature in the dark. The black solid at the bottom was removed by suction filtration, and the solvent was evaporated. It was dissolved in n-hexane and extracted with saturated brine, washed three times, and the organic phase was collected and dried with anhydrous Na_2SO_4. The organic solvent was evaporated and the resulting pale yellow solid was purified by silica gel chromatography (hexane as eluent) to give 4-trimethylsilylethynylbenzaldehyde as a white powder. ^{1}H NMR (500 MHz, $CDCl_3$) δ 10.00 (s, 1H), 7.81 (d, J = 8.2 Hz, 2H), 7.60 (d, J = 8.2 Hz, 2H), 0.27 (s, 9H). 4-trimethylsilylethynyl-benzaldehyde (5.3 g, 26 mmol) and redistilled pyrrole (2150 uL, 31 mmol) as raw materials in a 250 mL two-necked flask, add 70 mL of propionic acid, and stir well, the mixture was reacted at 140 °C under reflux for two days. After the reaction was completed, the precipitate was collected by cooling and suction filtration, and the obtained precipitate was fully washed with methanol until the washing solution was colorless, and dried to obtain TEPP-TMS [purple powder, 20.2% yield]. ^{1}H NMR (500 MHz, $CDCl_3$) δ 8.82 (s, 8H), 8.14 (d, J = 8.2 Hz, 8H), 7.87 (d, J = 8.4 Hz, 8H), 0.38 (s, 36H), -2.84 (s, 2H). Under argon atmosphere, 5 mg of TEPP-TMS

was dissolved in 8 mL of ultra-dry THF and stirred in an ice bath. After adding 1 mL of TBAF (1 M THF), the ligand was hydrolyzed for 20 min. The product was dissolved in dichloromethane, added with saturated brine, extracted and washed three times, dried over anhydrous magnesium sulfate to remove water, and the solvent was evaporated to obtain TEPP powder. Monomer hydrolysis is now used.

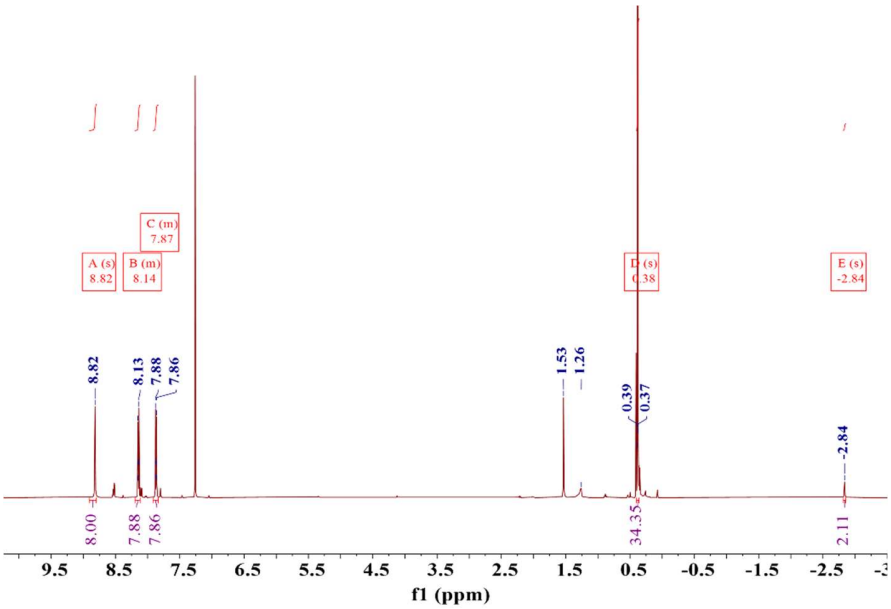

Figure S16. ^{1}H NMR of TEPP-TMS in $CDCl_3$ at R.T.

S5. Synthesis of polymers/Cu foil

Pretreatment of copper foil: The copper foil was cut into a size of 5.0 cm*0.8 cm, and folded into three folds of equal length. Then the copper foil was sonicated in 1 M HCl for 10 minutes and washed with ultrapure water five times, acetone for three times.

PDEB/Cu foil: The freshly treated copper foil was placed at the bottom of the three-necked flask, 10 mL of pyridine was added to immerse the copper foil, and 3.6 mg of 1,4-Bis[(trimethylsilyl)ethynyl]benzene (DEB-TMS) were hydrolyzed in the same procedure as HEB-TMS to obtain 1,4-diethynylbenzene (DEB), then the DEB monomer was dissolved in 5 mL of pyridine and placed in a constant-pressure separatory funnel. N_2 was introduced to drive out the dissolved air in the solvent by bubbling. When the reaction system was 80 °C, the monomer DEB was slowly added dropwise to the flask, and the reaction was carried out for 16 h in dark. Then taken out the copper foil, washed with acetone, ultrapure water and acetone three times in turn to obtain the poly-1,4-diacetylene benzene film, which generated in situ on the surface of the copper foil.

PTEB/Cu foil: It was the same synthesis method as PDEB/Cu foil, except that the 4.9 mg of 1,3,5-tris((trimethylsilyl)ethynyl)benzene (TEB-TMS) were hydrolyzed to obtain 1,3,5-Triacetylbenzene (TEB) monomer.

PHEB/Cu foil: It was the same synthesis method as PDEB/Cu foil, except that the 10 mg of HEB-TMS were hydrolyzed to obtain 1,2,3,4,5,6-hexaacetylene benzene (HEB) monomer.

PTFTEB/Cu foil: It was the same synthesis method as PDEB/Cu foil, except that 6mg of 1,3,5-(trimethylsilyl)ethynyl 2,4,6-trifluorobenzene was hydrolyzed to obtain 1,3,5-triethynyl-2,4,6-trifluorobenzene Fluorobenzene (TFTEB) as monomer.

PTEP/Cu foil: It was the same synthesis method as PDEB/Cu foil, except that 5mg of 2,4,6-tris((trimethylsilyl)ethynyl)pyridine was hydrolyzed to obtain 2,4,6-triethynylpyridine (TEP) instead of DEB monomer.

PTEPA/Cu foil: It was the same synthesis method as PDEB/Cu foil, except that 4mg of tris(4-((trimethylsilyl)ethynyl)phenyl)amine was hydrolyzed to obtain 2,4,6-triethynylpyridine (TEPA) instead of DEB monomer.

PTETZ/Cu foil: It was the same synthesis method as PDEB/Cu foil, except that 8mg of 2,4,6-tris(4-((trimethylsilyl)ethynyl)phenyl)-1,3,5-triazine was hydrolyzed to obtain 2,4,6-tris(4-ethynylphenyl))-1,3,5-triazine (TETZ) instead of DEB monomer.

PTEPP/Cu foil: It was the same synthesis method as PDEB/Cu foil, except that 2mg of 5,10,15,20-tetrakis(4-((trimethylsilyl)ethynyl)phenyl)porphyrin (TEPP-TMS) was hydrolyzed to obtain 5,10,15,20-tetrakis(4-ethynylphenyl)porphyrin (TEPP) instead of DEB monomer.

py/Cu foil: The freshly treated copper foil was placed at the bottom of the three-necked flask, 10 mL of pyridine was added to immerse the copper foil, 5 mL pyridine were placed in a constant-pressure separatory funnel. The N_2 was introduced to drive out the dissolved air in the solvent by bubbling. After the copper foil and the pyridine solution were kept at 80 °C for 10 h in dark, the pyridine (in a constant-pressure separatory funnel) was slowly dropwise added to the flask, and the reaction was carried out for 5 h. After taken out the copper foil, washed it with acetone, ultrapure water and acetone three times in turn to obtain the py/Cu foil.

S6. Preparation of working electrode for flow cell

Electrodeposition of Cu electrode: The backside of the gas diffusion layer was covered with PTFE tape to avoid copper deposition. The reference electrode was saturated Ag/AgCl electrode, and the counter electrode was graphite sheet. The electrodeposition was carried out in 1 M HCl and 1M CuCl at a constant current density of -10 mA cm^{-2} until a final deposition charge of 2 C cm^{-2} was reached. Then the as-prepared electrode was washed with water.

PTFTEB-CuCl: 2 mg CuCl and 2 ml pyridine were added in the three-necked flask, and 10 mg of 1,3,5-(trimethylsilyl)ethynyl 2,4,6-trifluorobenzene was hydrolyzed to obtain 1,3,5-triethynyl-2,4,6-trifluorobenzene Fluorobenzene (TFTEB) as monomer. The monomer was dissolved in 2 mL of pyridine and placed in a constant-pressure separatory funnel. N_2 was introduced to drive out the dissolved air in the solvent by bubbling. When the reaction system was 80 °C, the monomer TFTEB was slowly added dropwise to the flask, and the reaction was carried out for 16 h in dark. Then the brown precipitates were washed twice with chloroform and acetone, respectively.

Electrodeposition Cu/PTFTEB-CuCl: The PTFTEB-CuCl were dispersed in isopropanol by sonicating. Typically, 0.03 mg cm^{-2} of the PTFTEB-CuCl was drop-casted on the GDL. The modified GDL using the same method of electrodeposition Cu to fabricate electrodeposition Cu/PTFTEB-CuCl.

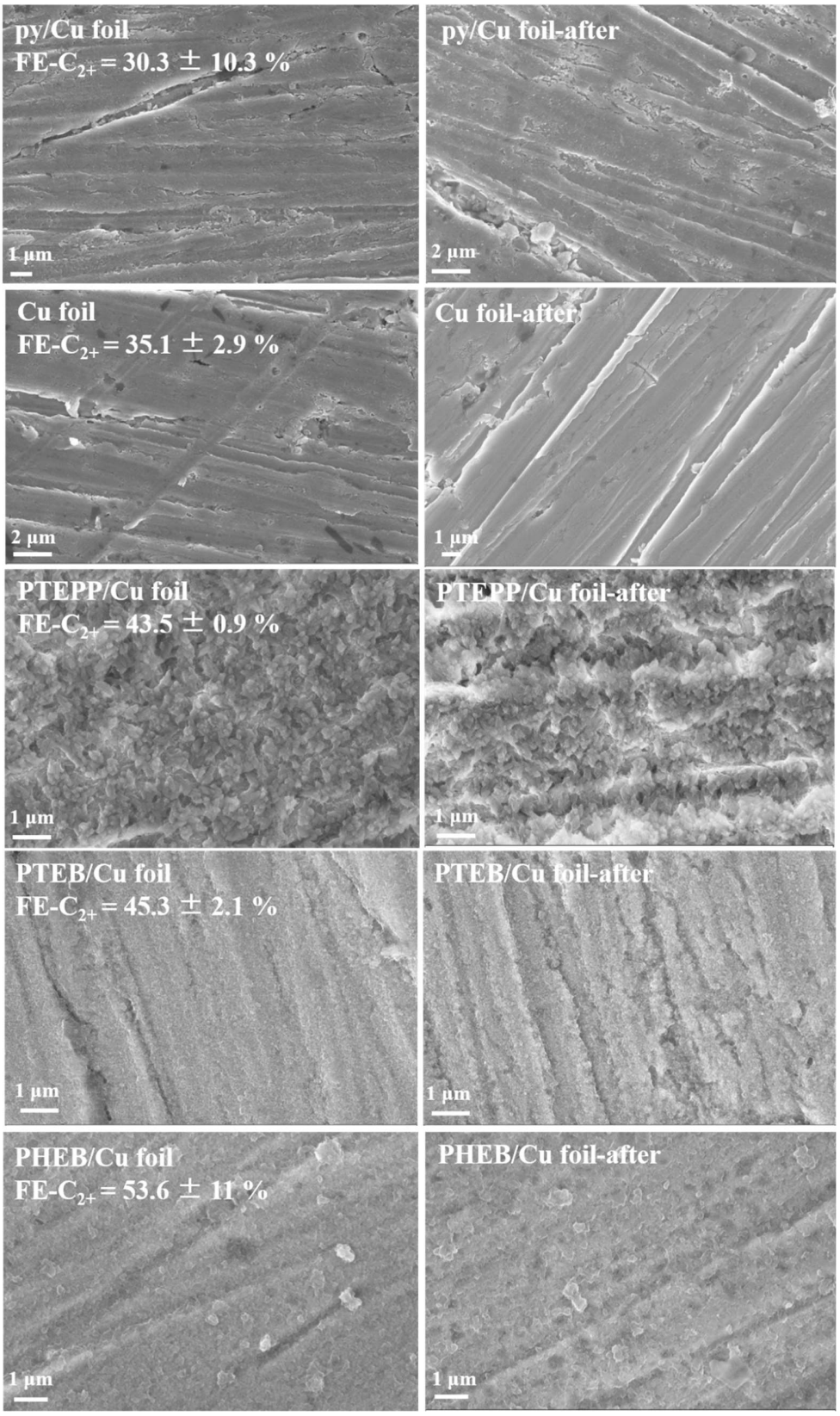
py/Cu foil
FE-C2+ = 30.3 ± 10.3 %
1 μm
py/Cu foil-after
2 μm
Cu foil
FE-C2+ = 35.1 ± 2.9 %
2 μm
Cu foil-after
1 μm
PTEPP/Cu foil
FE-C2+ = 43.5 ± 0.9 %
1 μm
PTEPP/Cu foil-after
1 μm
PTEB/Cu foil
FE-C2+ = 45.3 ± 2.1 %
1 μm
PTEB/Cu foil-after
1 μm
PHEB/Cu foil
FE-C2+ = 53.6 ± 11 %
1 μm
PHEB/Cu foil-after
1 μm

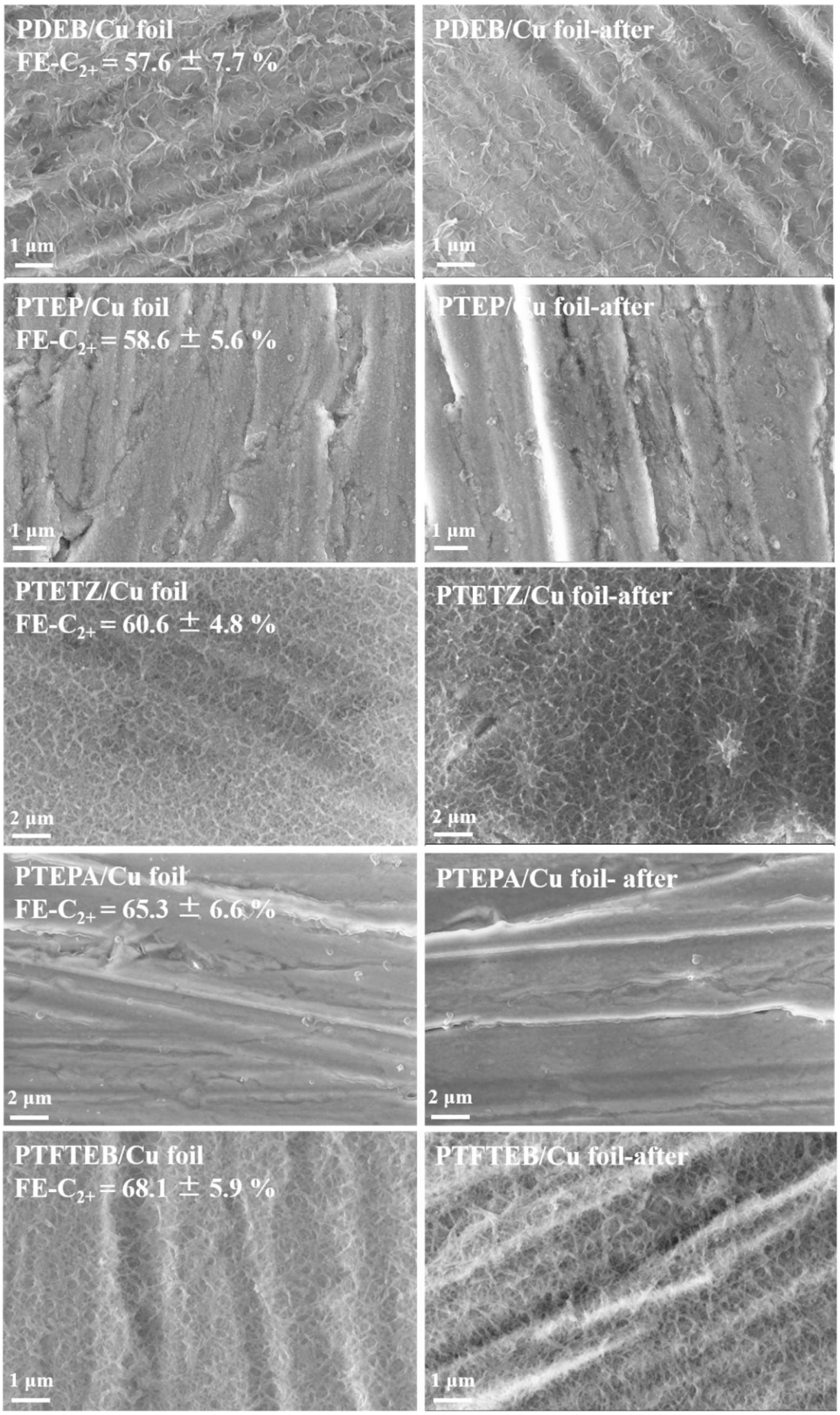

Figure S17. SEM images of Cu foil, modified polymer/Cu foils, and control sample py/Cu foil before and after electrocatalytic CO_2 reduction.

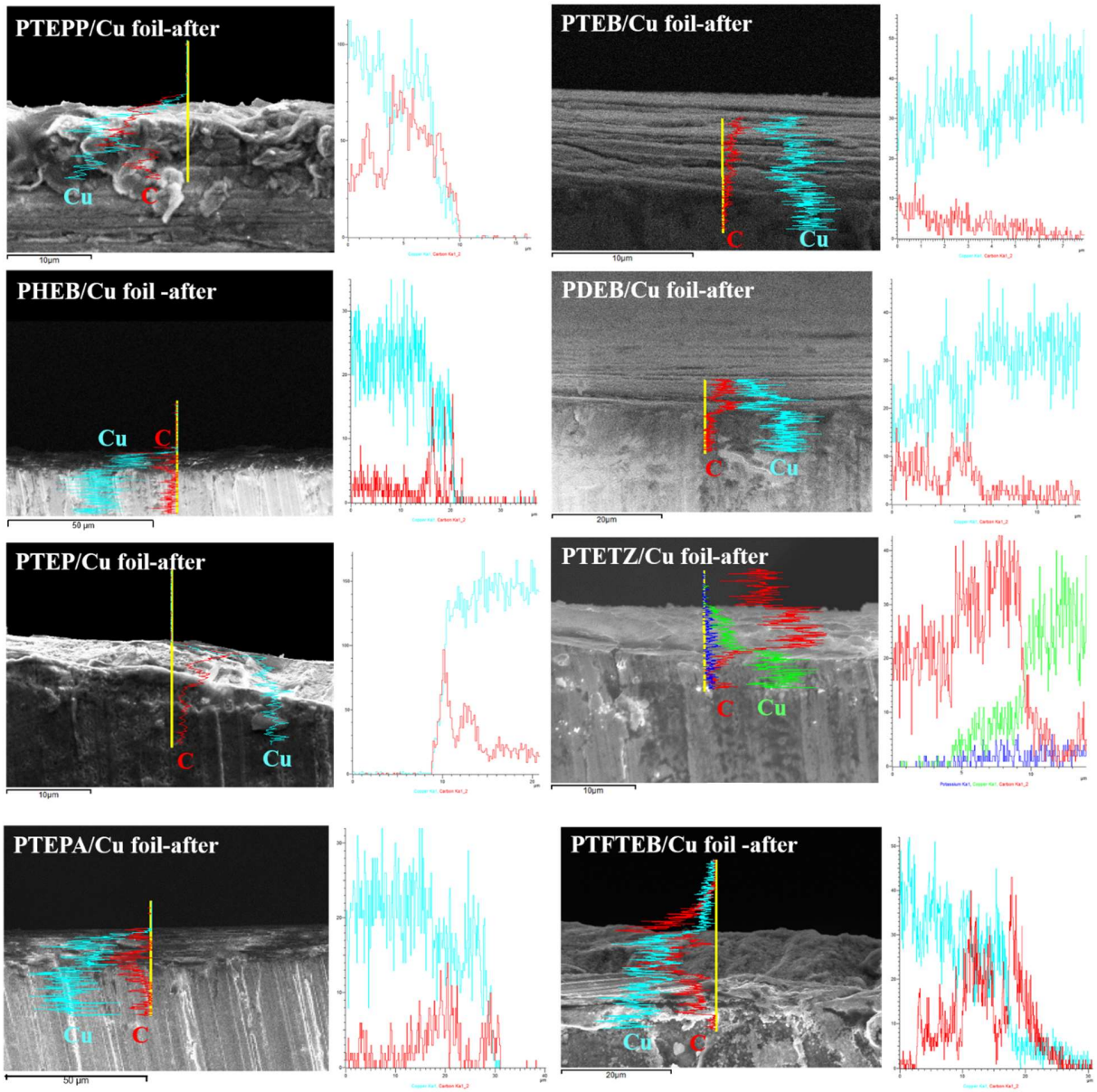

Figure S18. Cross section SEM images and EDX line scan of polymer/Cu foil after electrocatalytic CO_2 reduction.

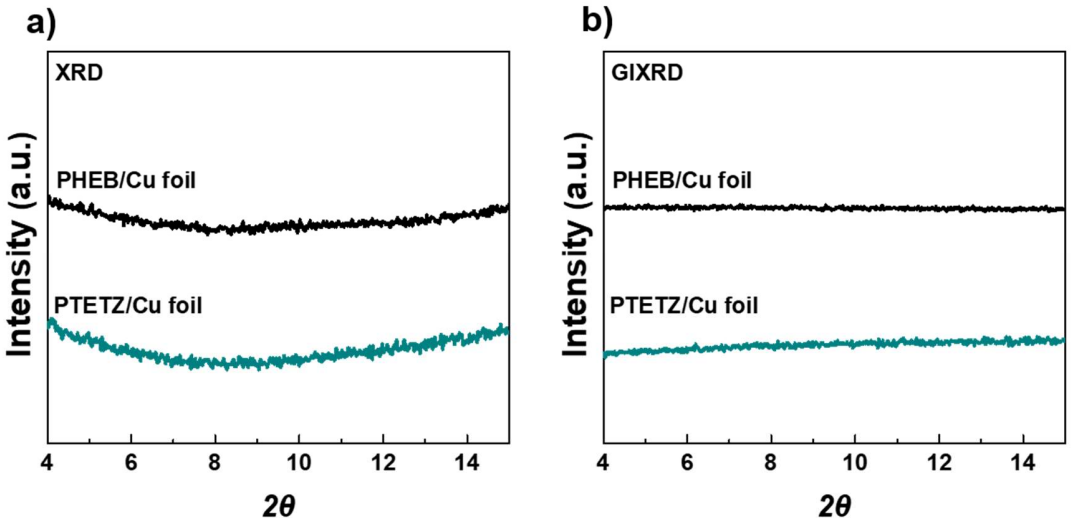

Figure S19. PXRD and GIXRD pattern of PTETZ/Cu foil and PHEB/Cu foil.

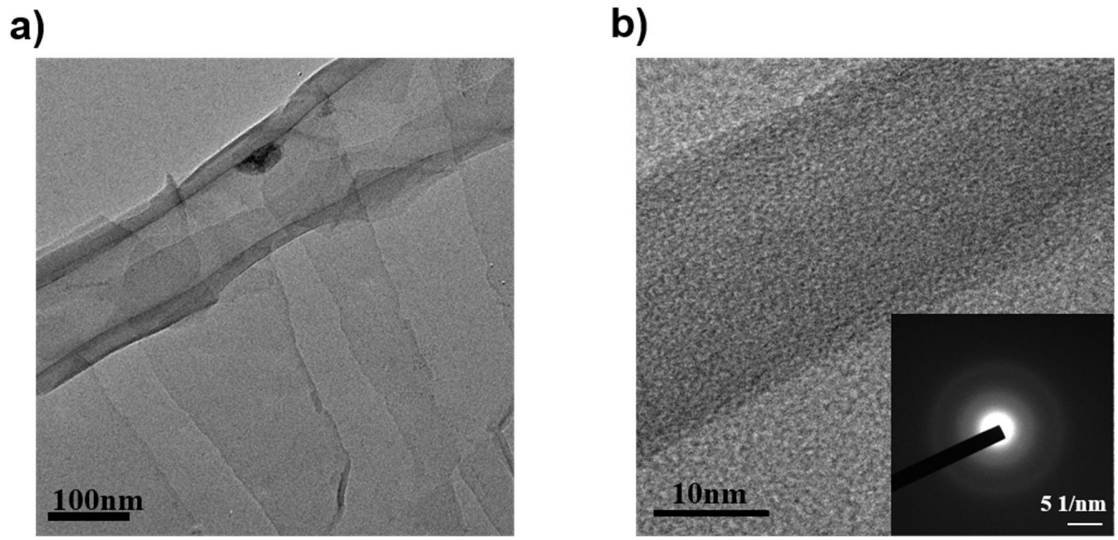

Figure S20. HRTEM images of PTETZ. The inset in b) is the SAED pattern of PTETZ. Polymer films were stripped from Cu foil using $FeCl_3$ saturated solution, and washed with H_2O and ethanol.

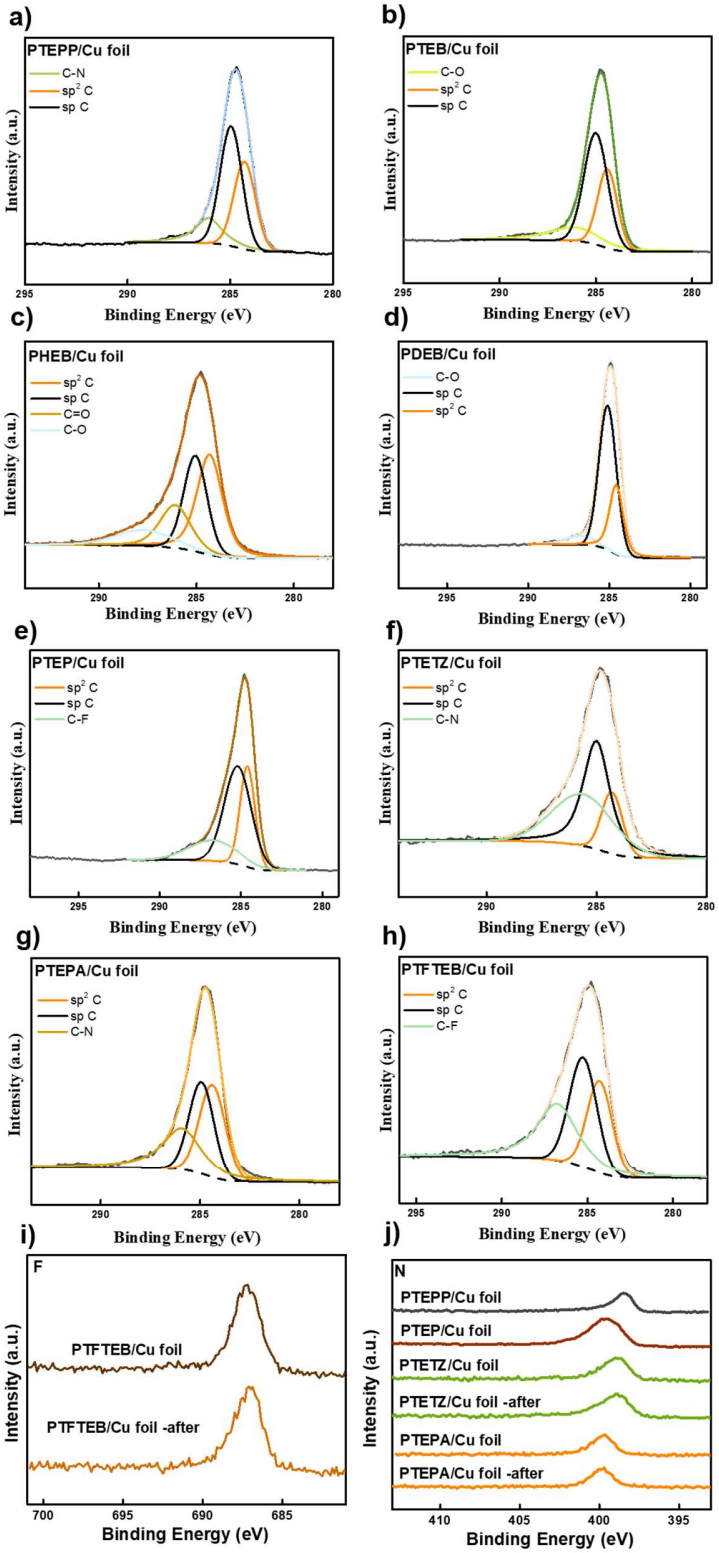

Figure S21. a-h) XPS spectra of C 1s for polymer/Cu foil, i) XPS spectra of F 1s for PTFTEB/Cu foil before and after electrolysis, j) XPS spectra of N 1s for four samples containing N element, and PTEPA/Cu foil, PTETZ/Cu foil after electrolysis.

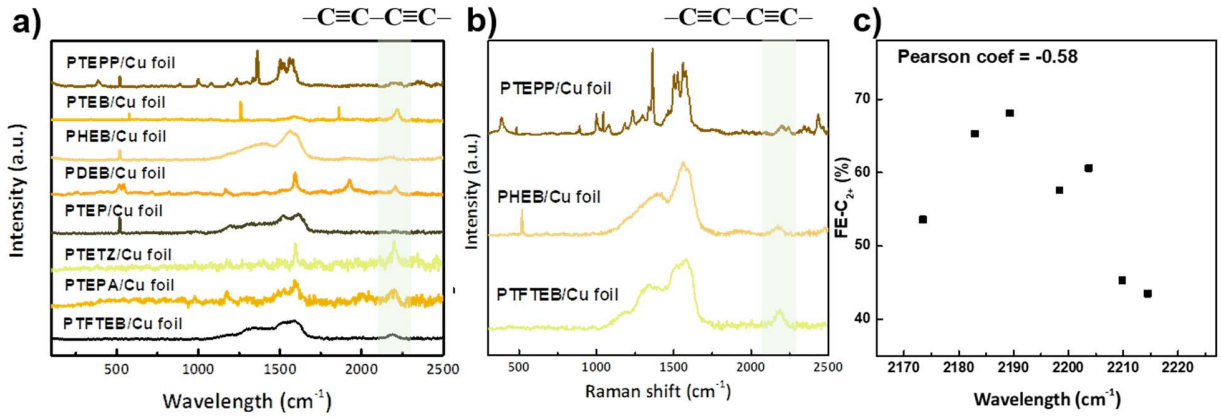

Figure S22. a) Raman spectra of alkyne conjugated polymer films. b) Raman spectra of PTEPP/Cu foil, PHEB/Cu foil and PTFTEB/Cu foil. c) Relationship between the wavelength of butadiyne linkages and C_{2+}-FE of polymer/Cu foil.

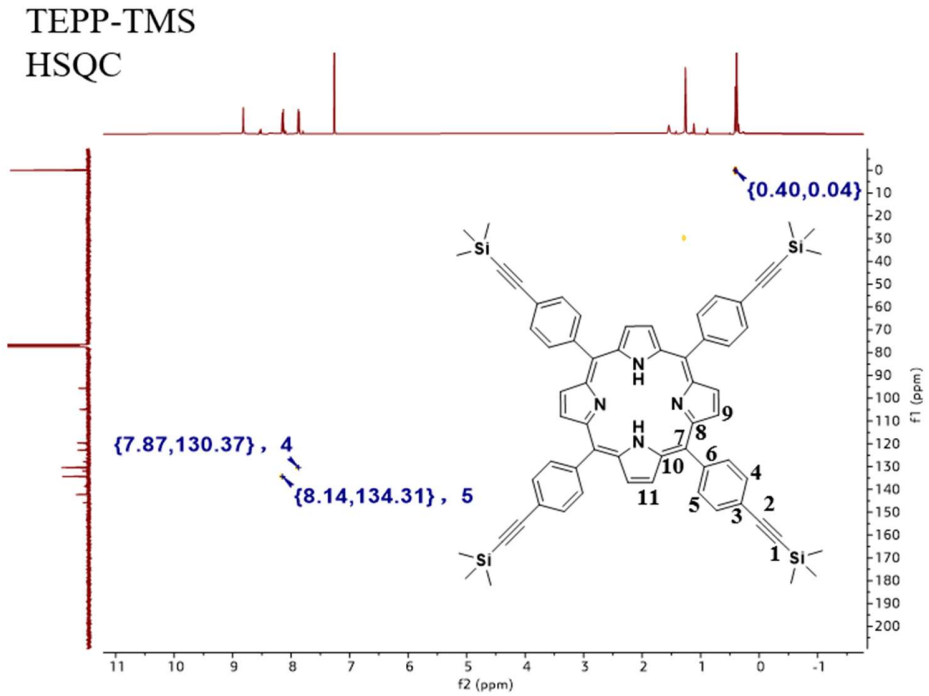

TEPP-TMS
HMBC

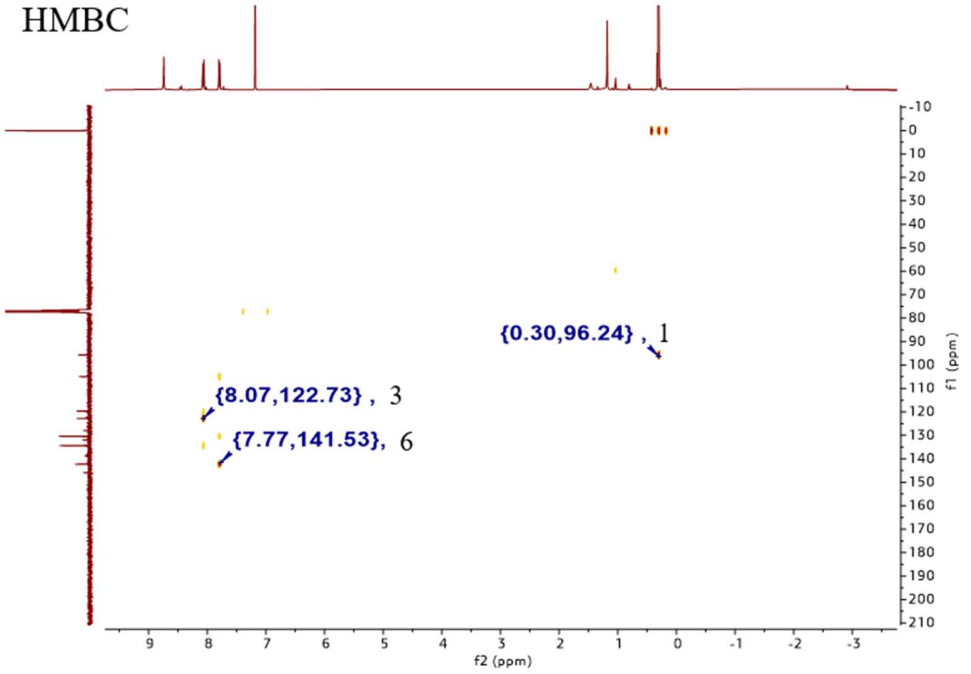

TEPP-TMS
^{13}C NMR

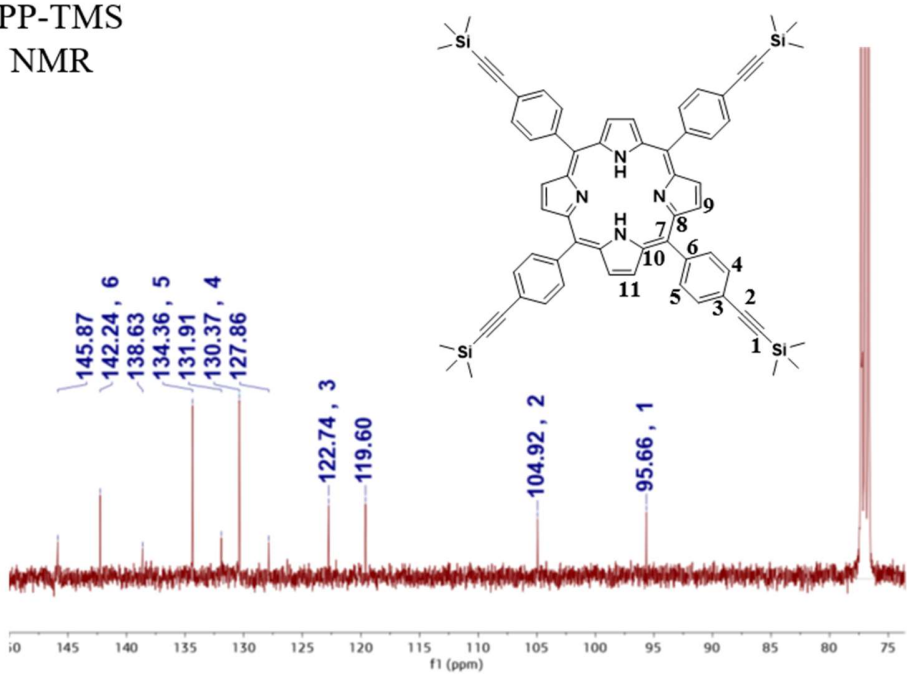

TEB-TMS
HSQC

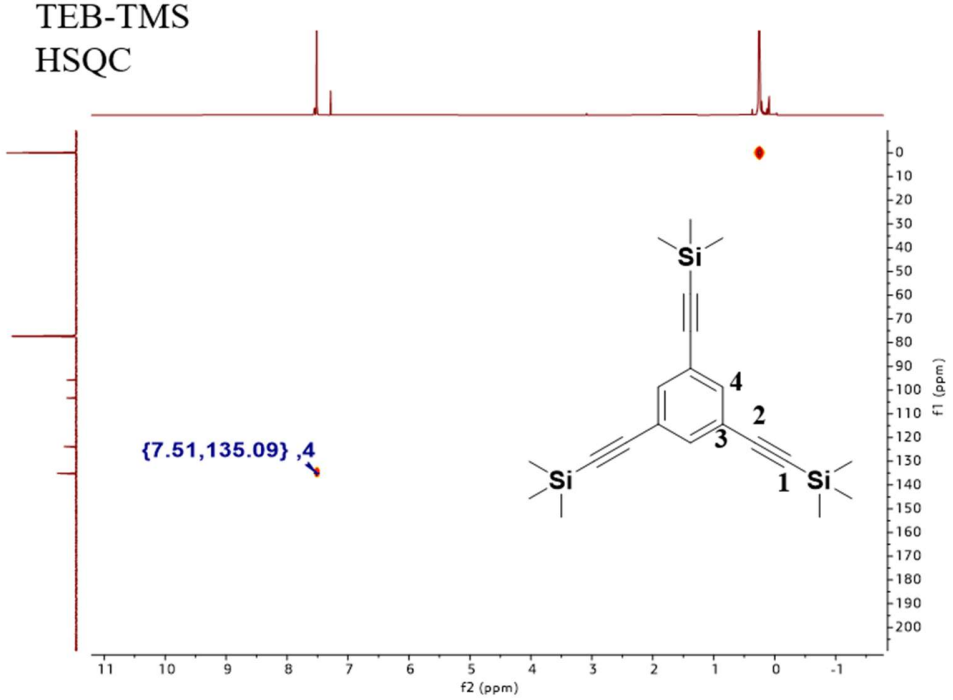

TEB-TMS
HMBC

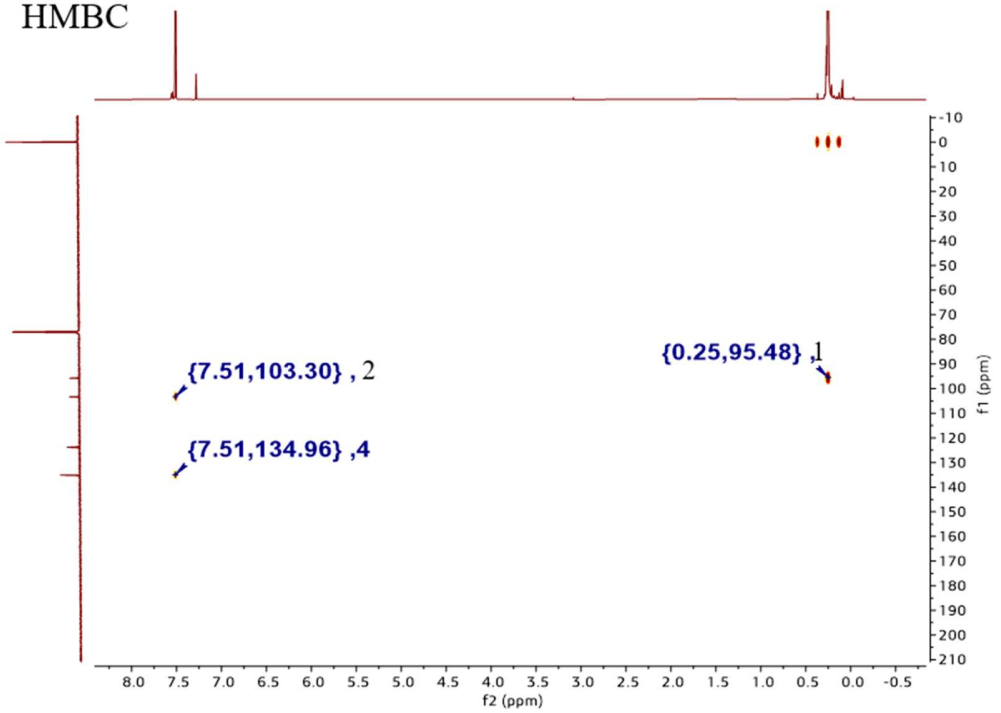

TEB-TMS
^{13}C NMR

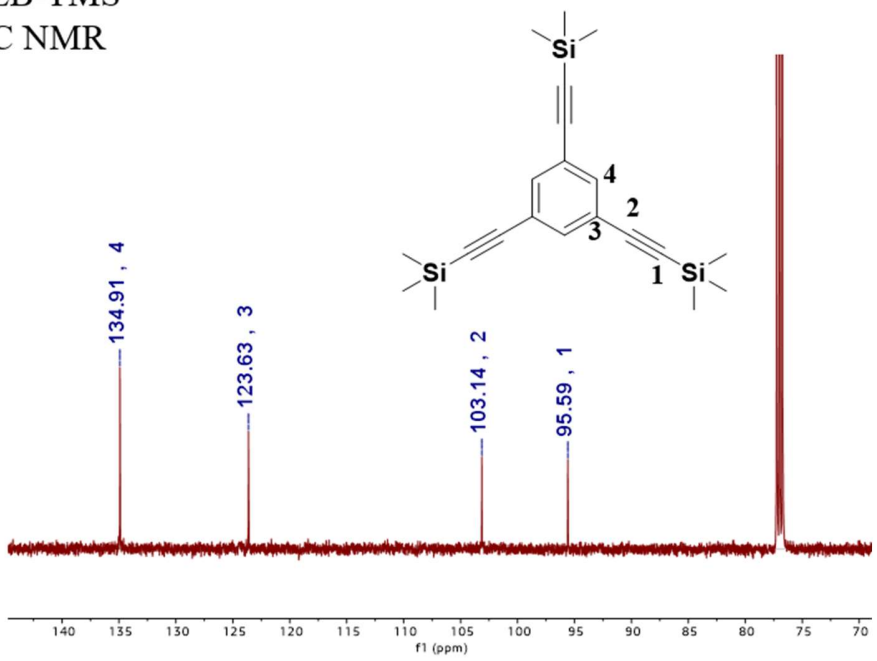

HEB-TMS
HMBC

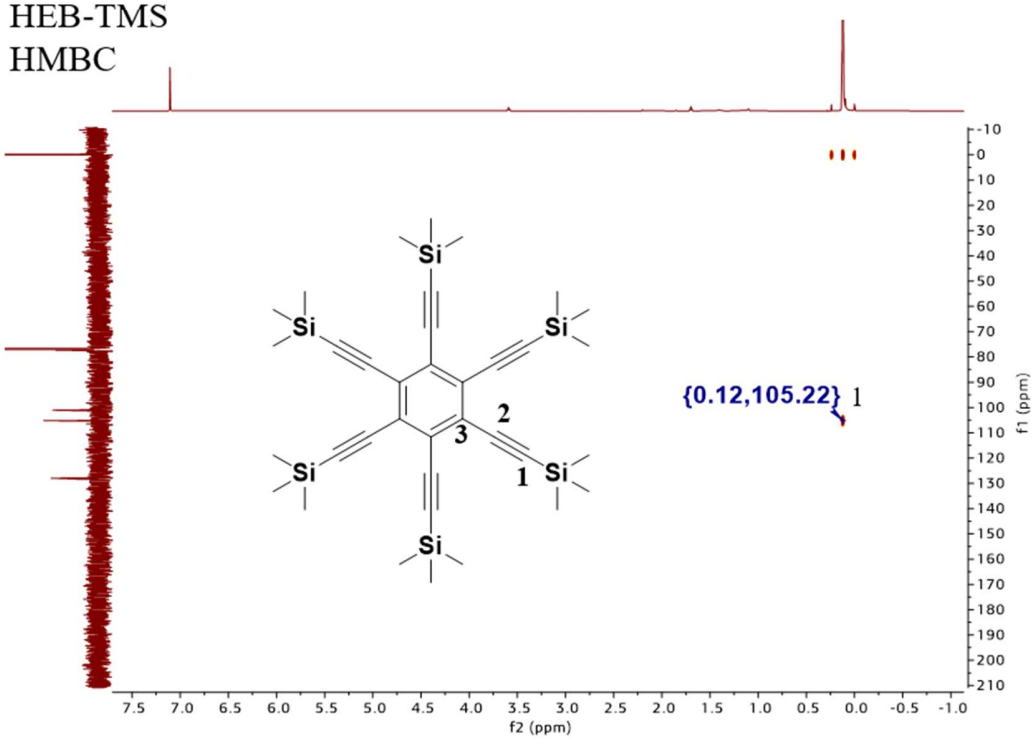

HEB-TMS

^{13}C NMR

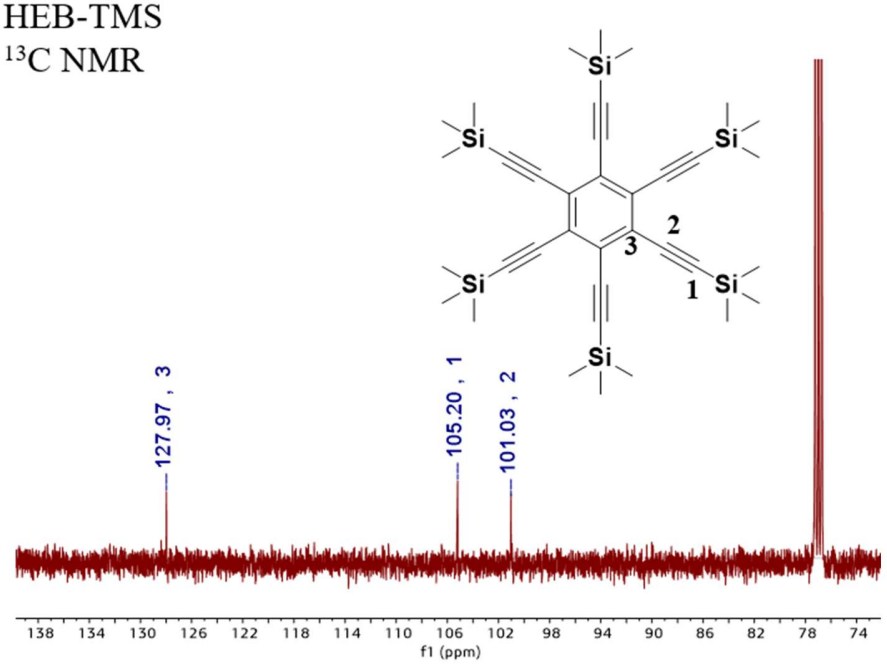

DEB-TMS

HSQC

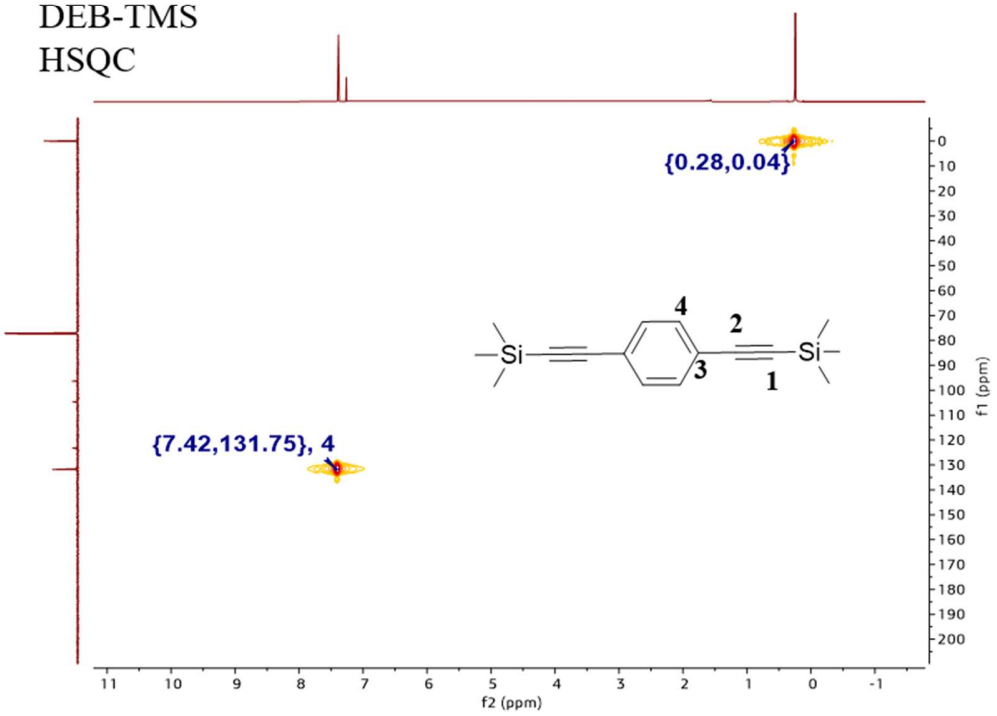

DEB-TMS
HMBC

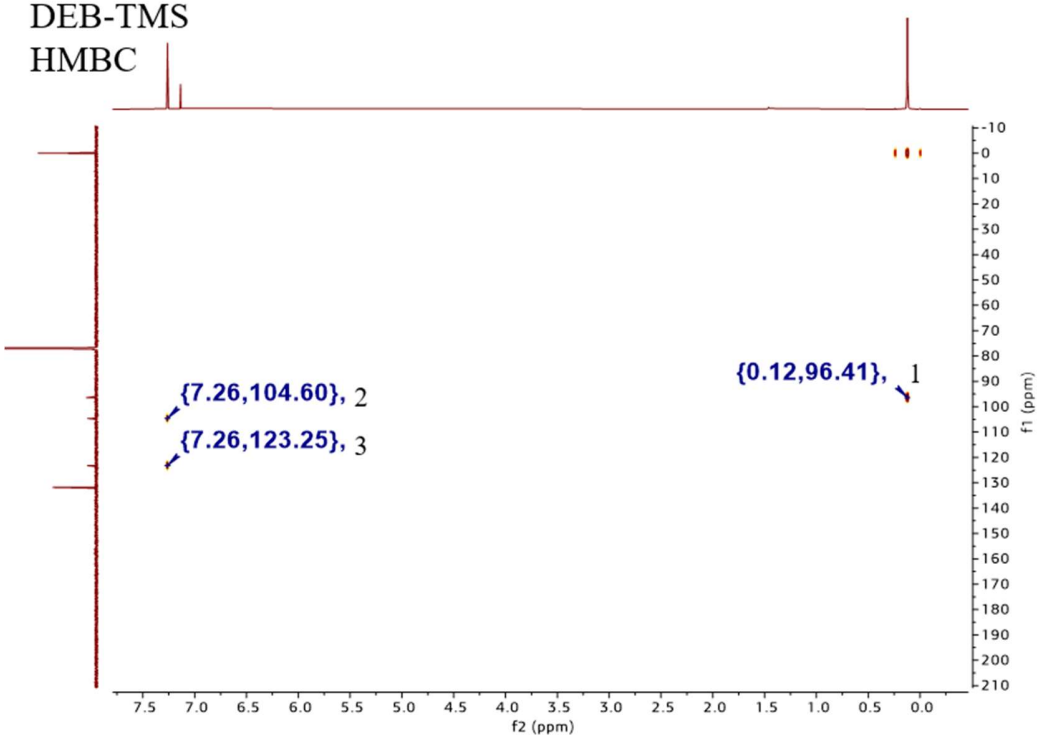

DEB-TMS
^{13}C NMR

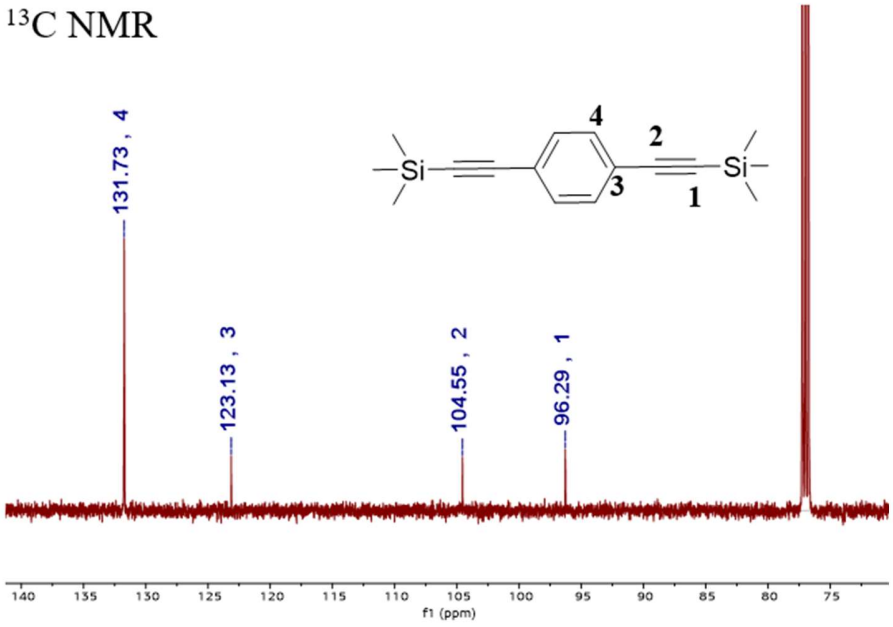

TEP-TMS
HSQC

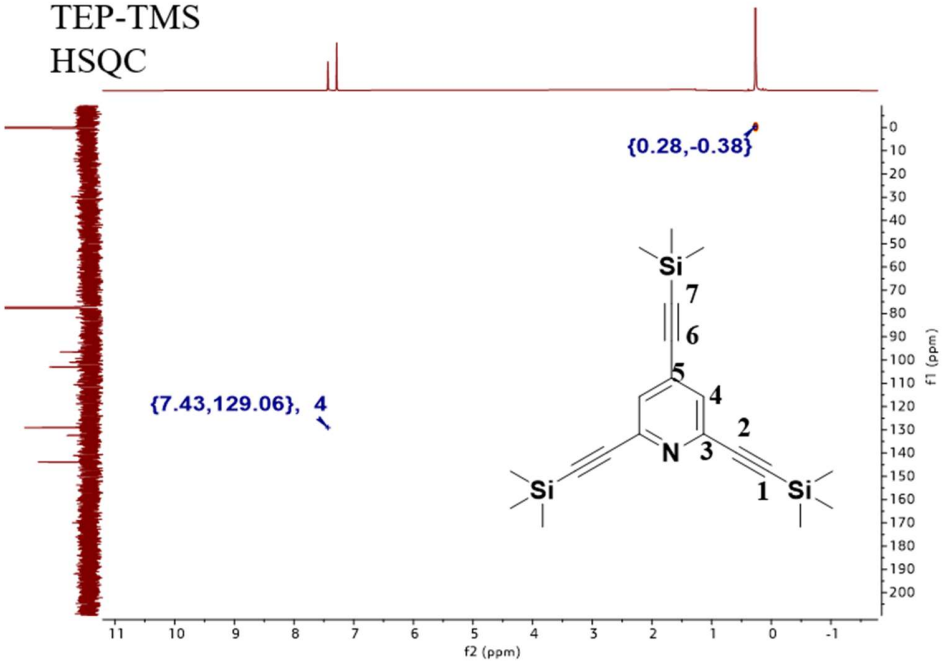

TEP-TMS
HMBC

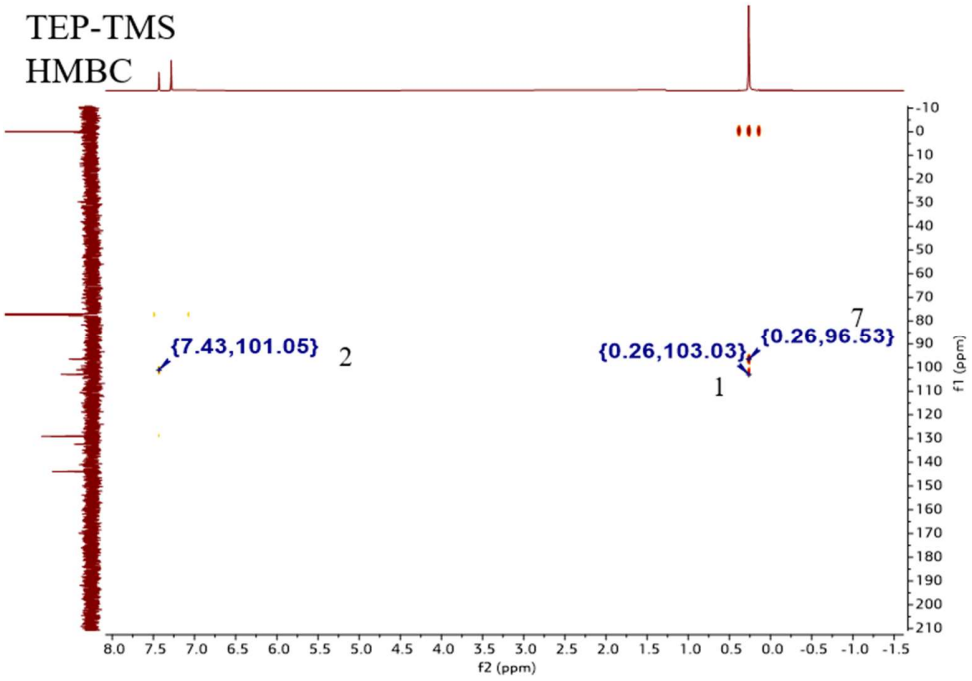

TEP-TMS
^{13}C NMR

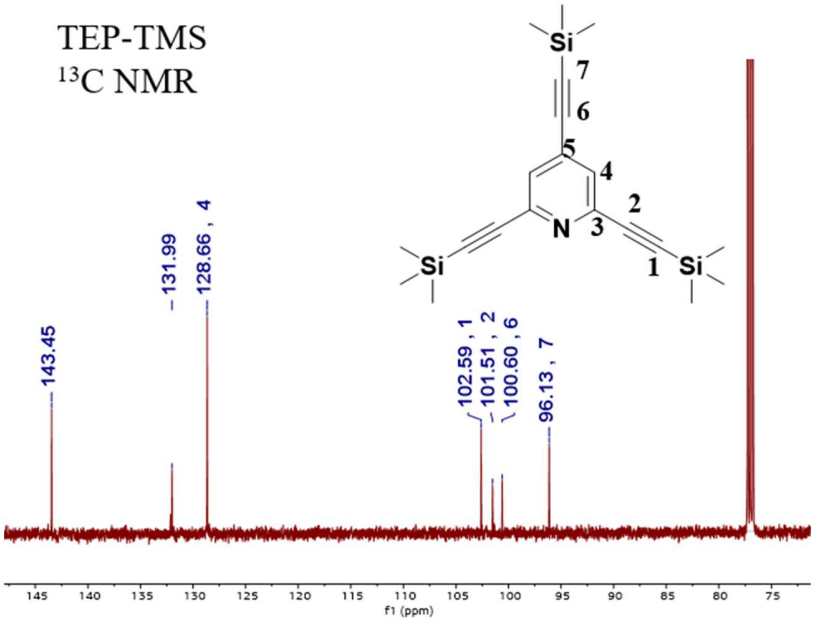

TETZ-TMS
HSQC

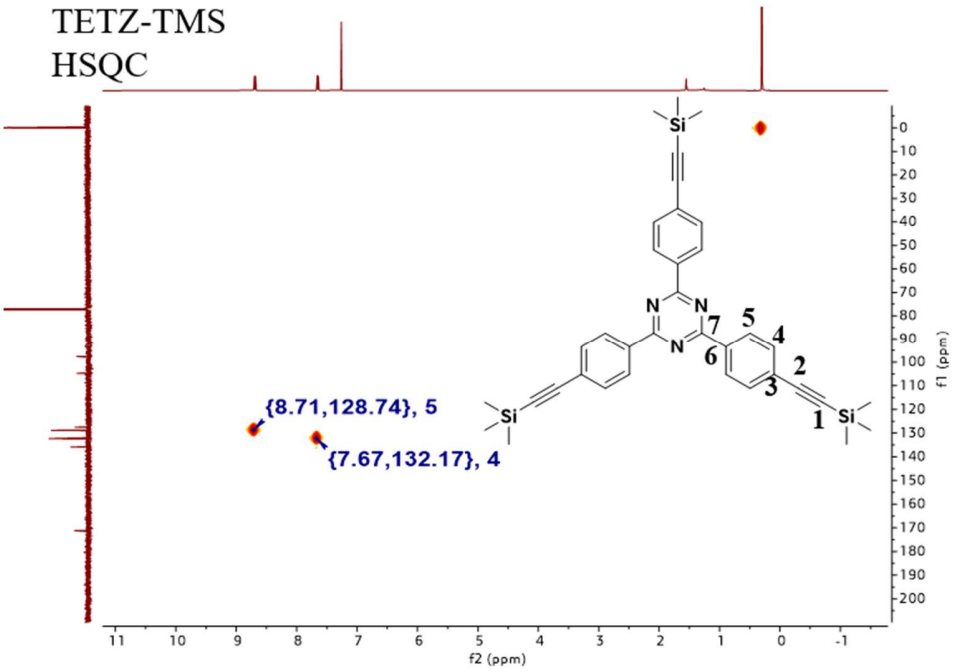

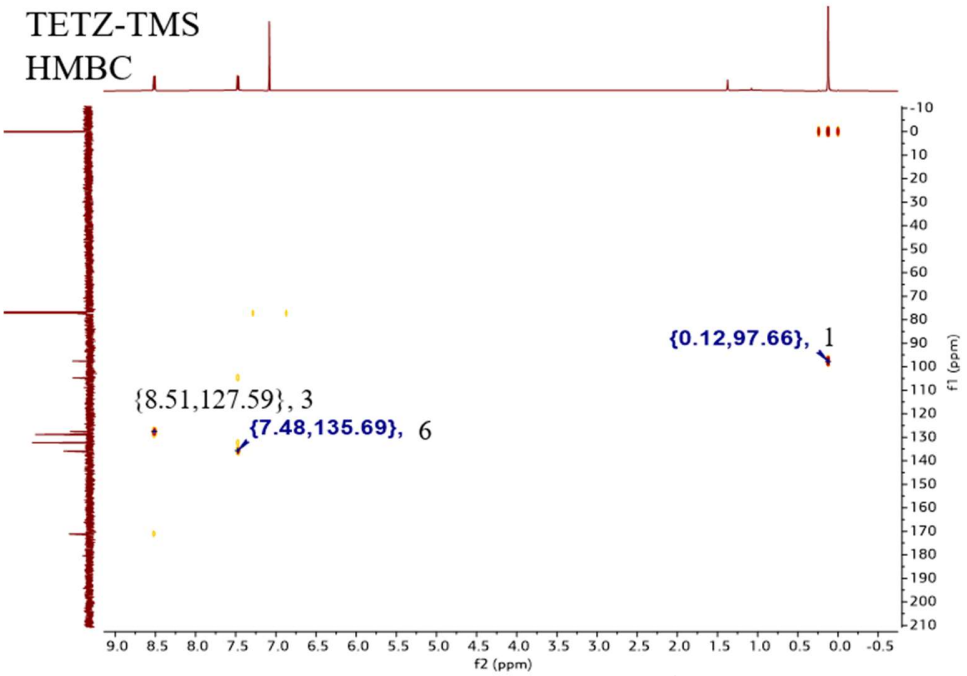
TETZ-TMS
HMBC
{0.12,97.66}, 1
{8.51,127.59}, 3
{7.48,135.69}, 6
f2 (ppm)
f1 (ppm)

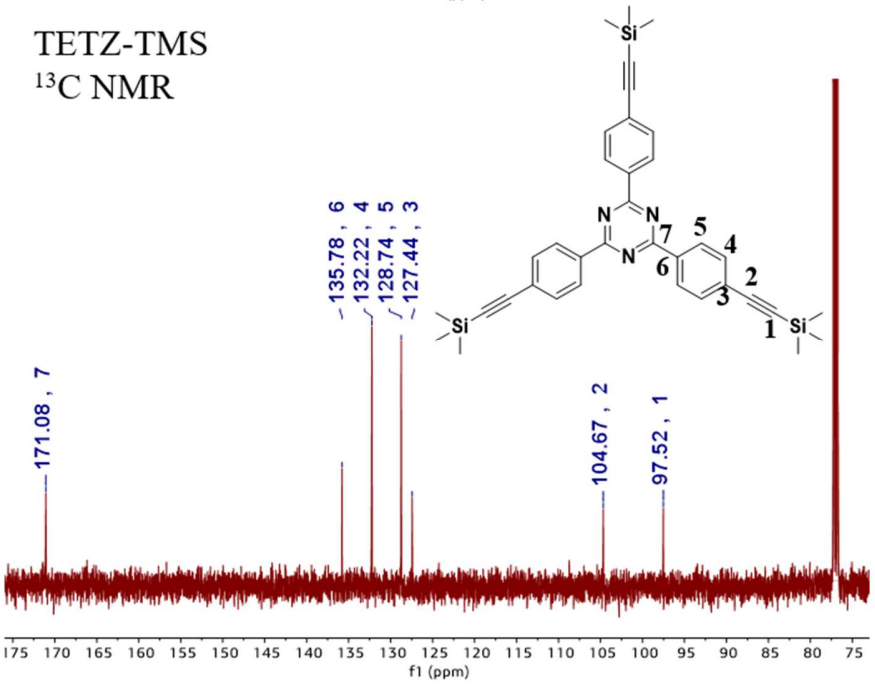
TETZ-TMS
13C NMR
135.78 , 6
132.22 , 4
128.74 , 5
127.44 , 3
171.08 , 7
104.67 , 2
97.52 , 1
Si
N
1
2
3
4
5
6
7
f1 (ppm)

TEPA-TMS
HSQC

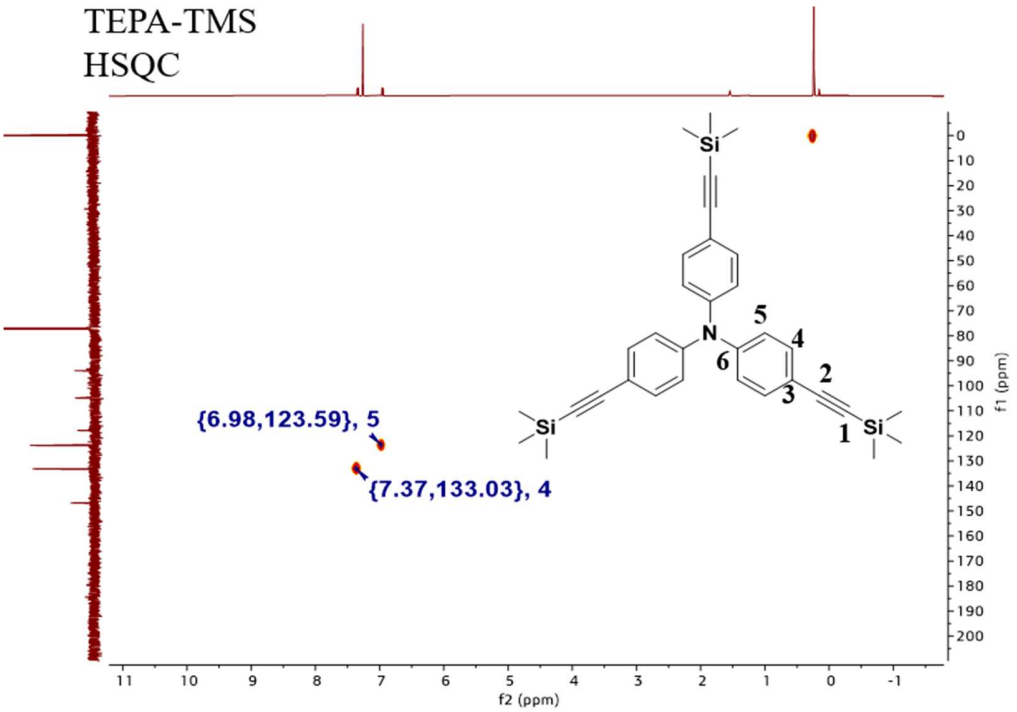

TEPA-TMS
HMBC

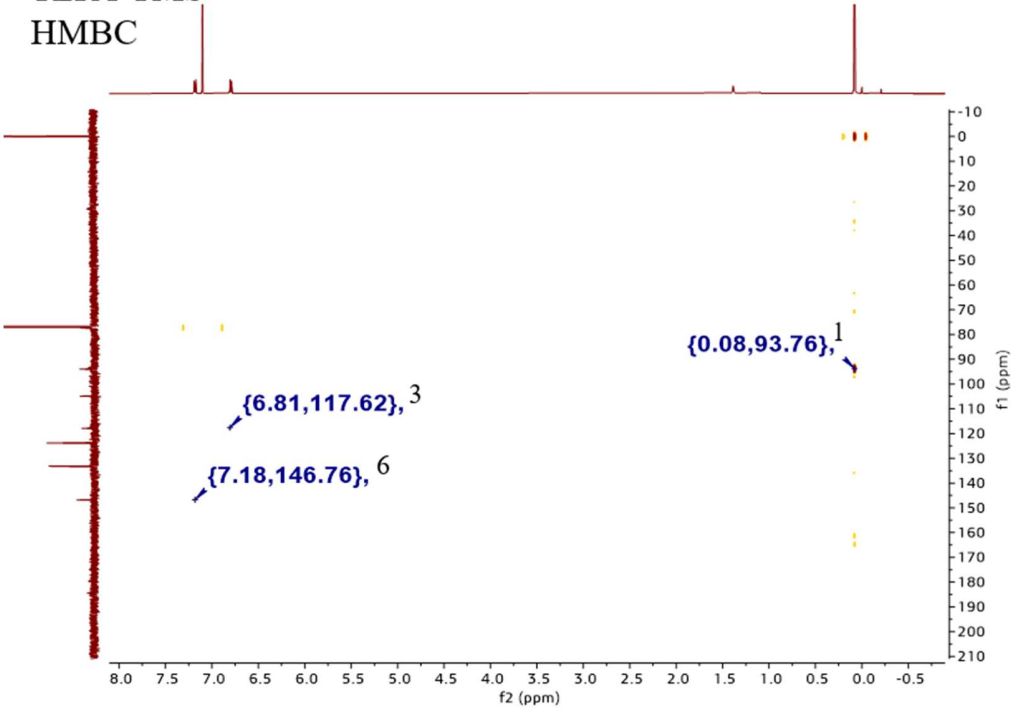

TEPA-TMS
^{13}C NMR

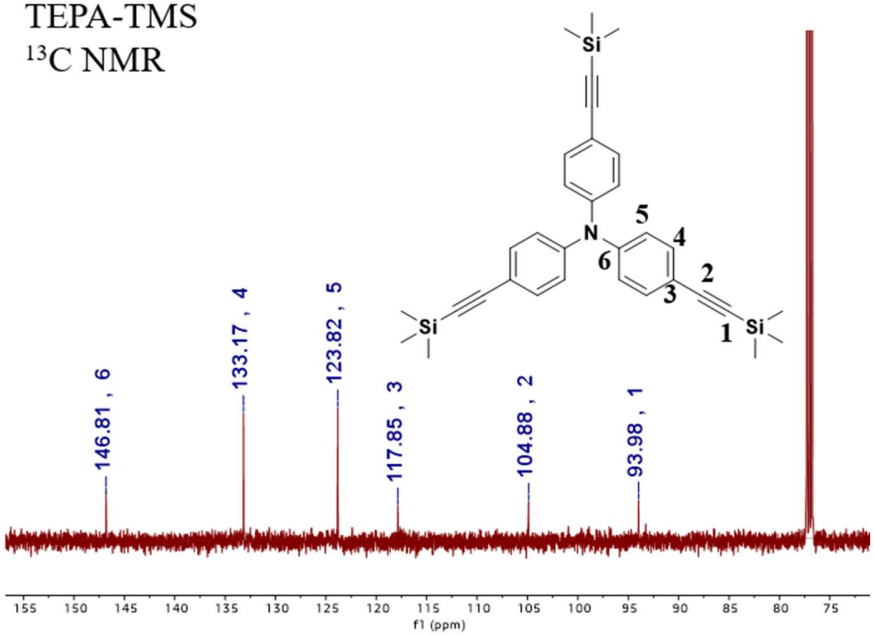

TFTEB-TMS
HMBC

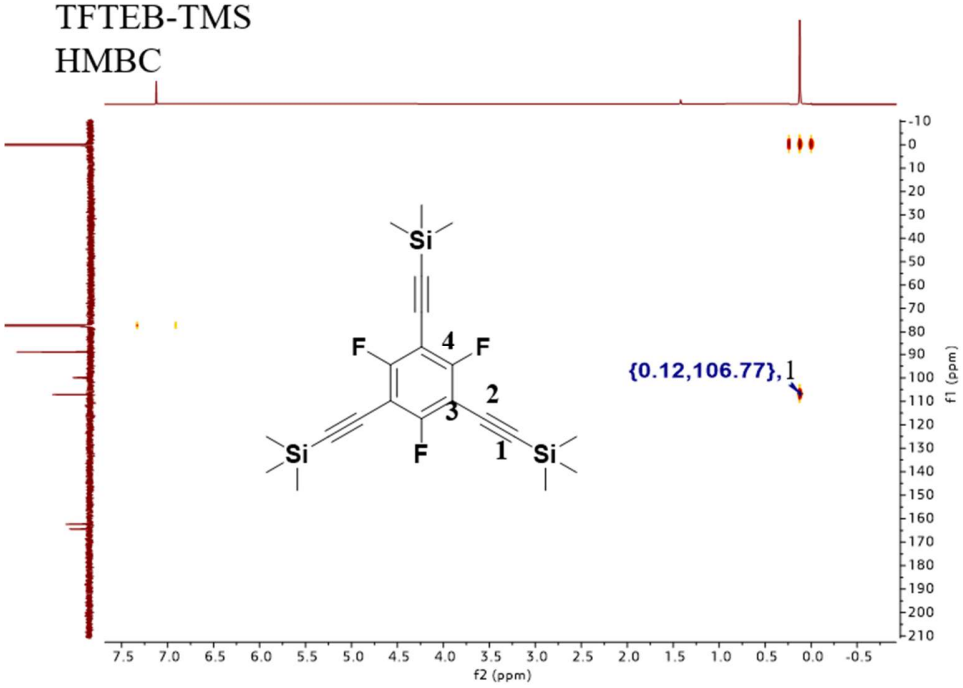

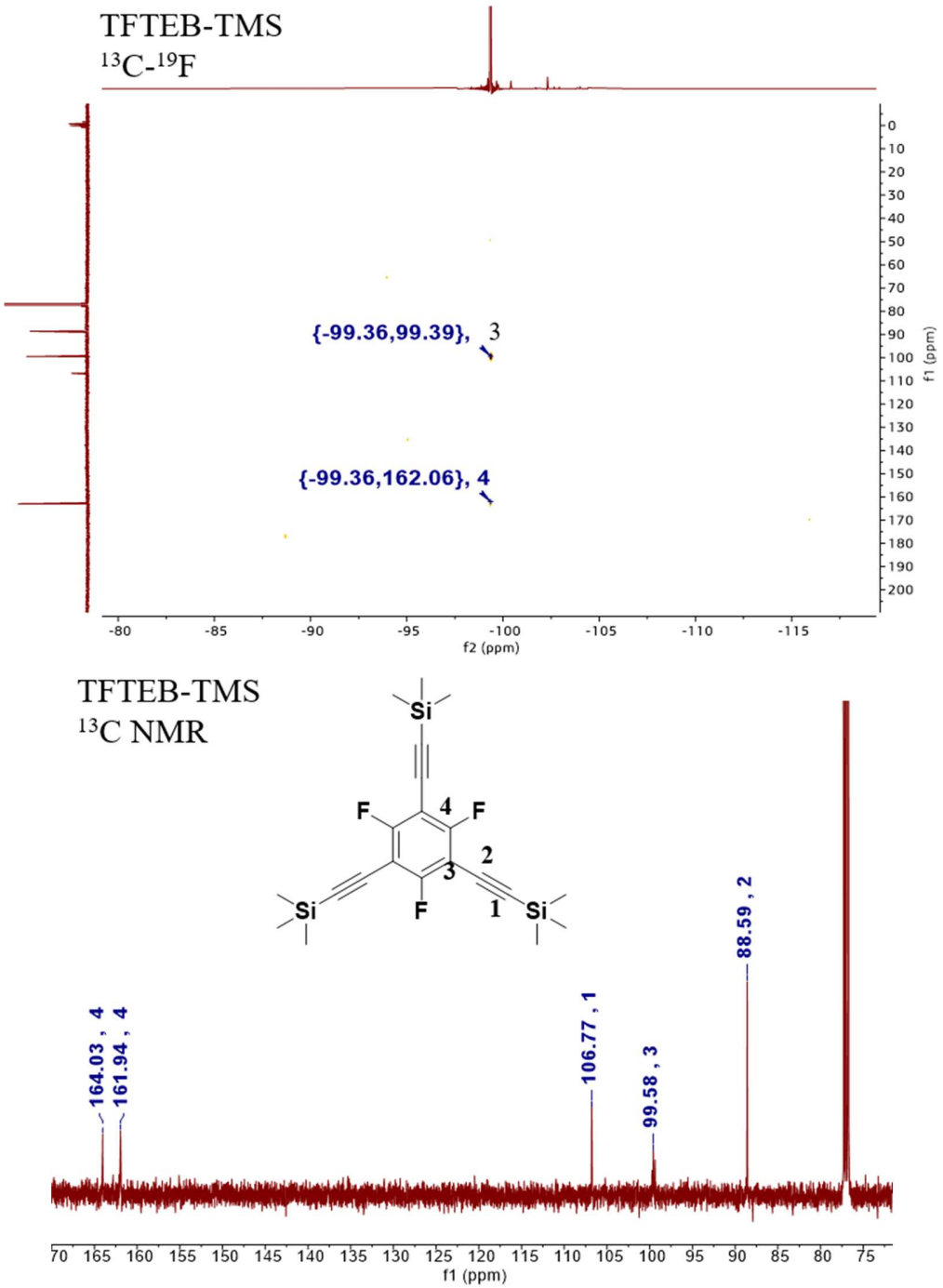

Figure S23. 2D ^{1}H-^{13}C HSQC (Heteronuclear Single-Quantum Correlation spectroscopy), HMBC (Heteronuclear Multiple Bond Coherence spectroscopy) NMR, and ^{13}C NMR spectra of monomer-TMS. COSY ^{13}C-^{19}F NMR spectrum of TFTEB-TMS.

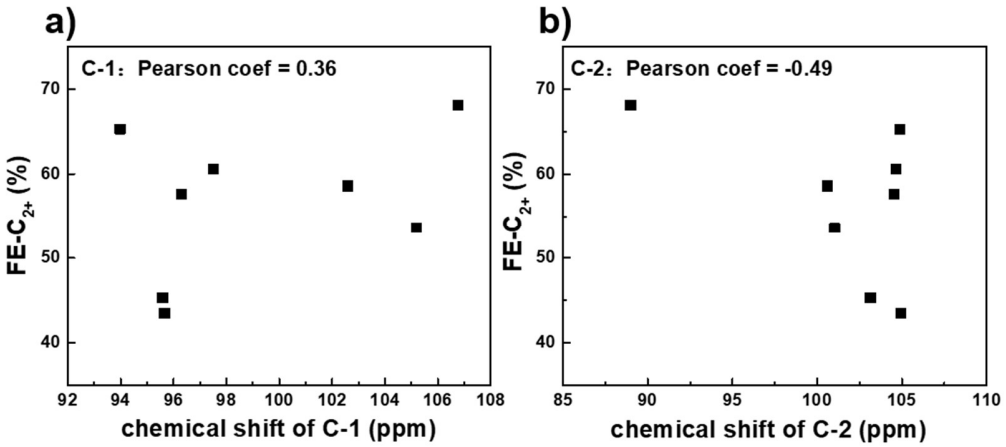

Figure S24. Relationship between the ^{13}C-NMR chemical shift of alkyne group for monomer-TMS and C_{2+}-FE of polymer/Cu foil.

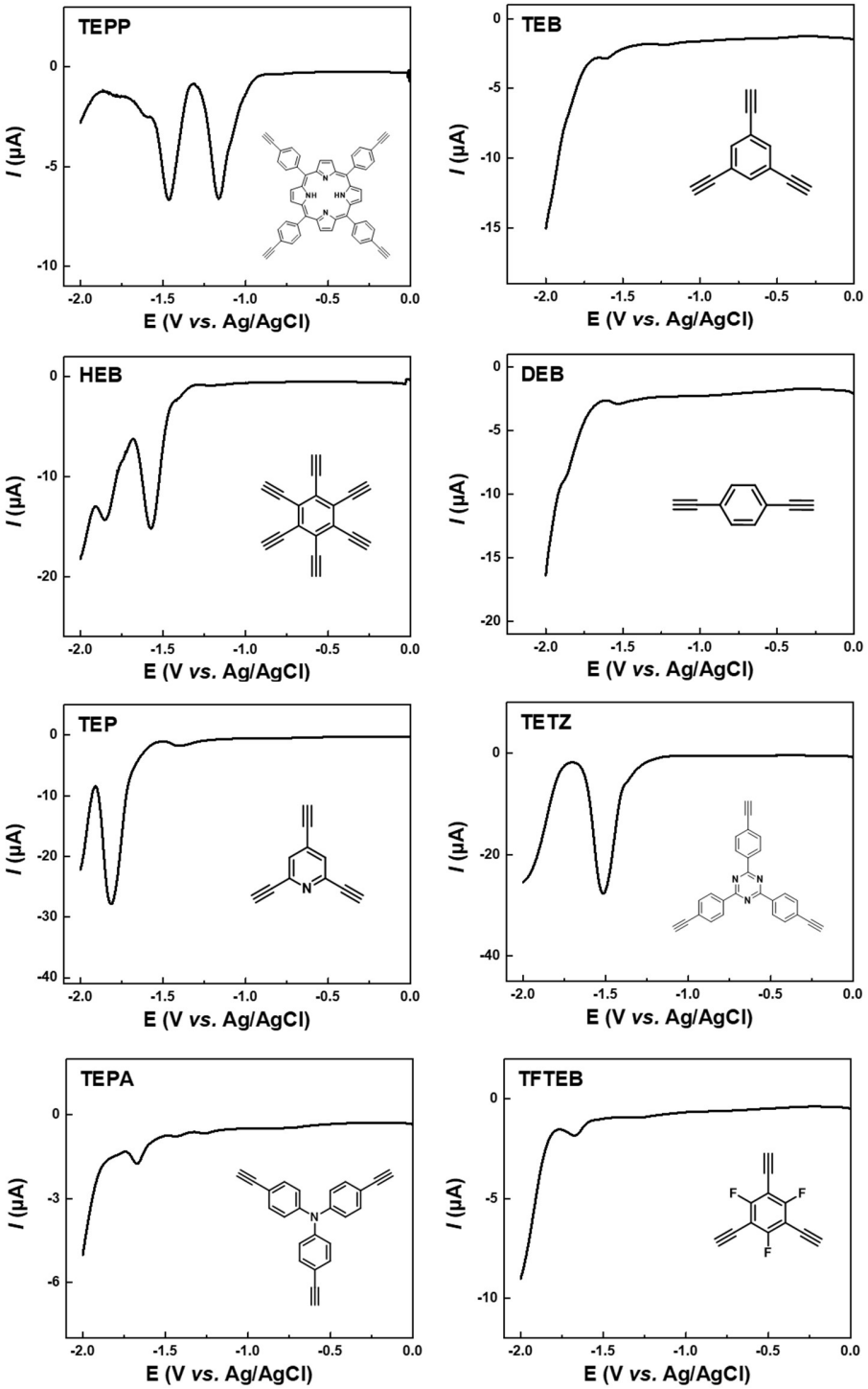

Figure S25. Differential pulse voltammetry (DPV) curves of 5 mM monomers (which were hydrolyzed from monomer-TMS) in N_2-saturated 0.1 M Bu_4NFP_6/CH_2Cl_2.

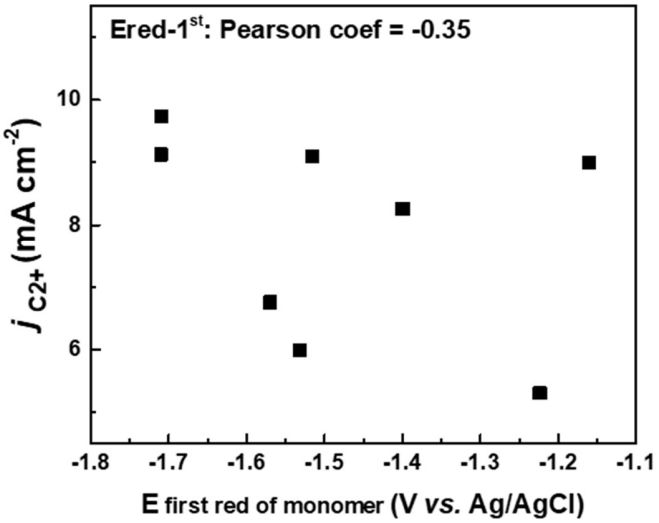

Figure S26. Relationship between the first reduction potential of monomers and partial curret density of C_{2+} (j C_{2+}) for corresponding polymer/Cu foil.

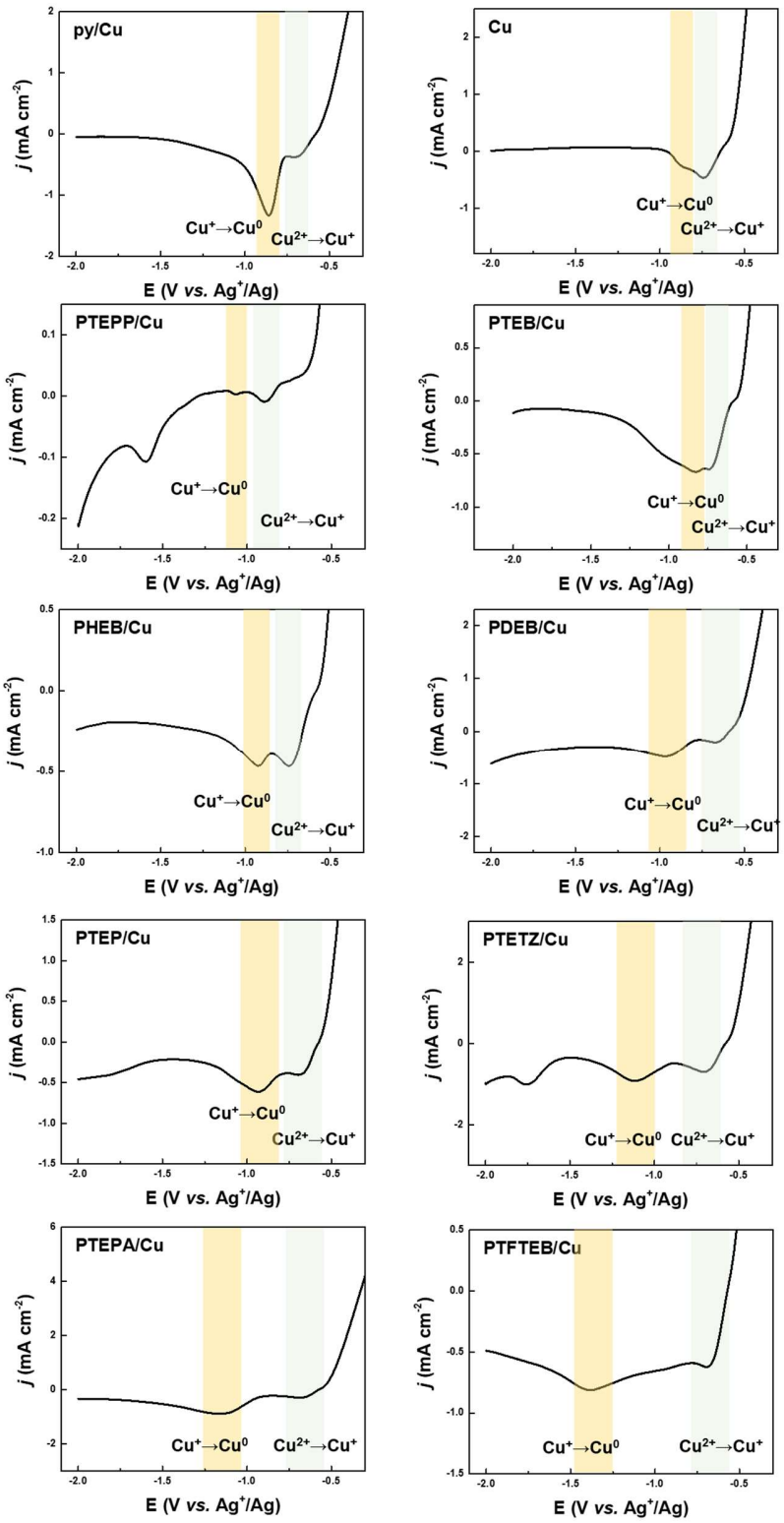

Figure S27. Cyclic voltammetry (CV) curves of polymer/Cu foil, py/Cu foil and Cu foil in N_2-saturated 0.1 M Bu_4NFP_6/CH_3CN.

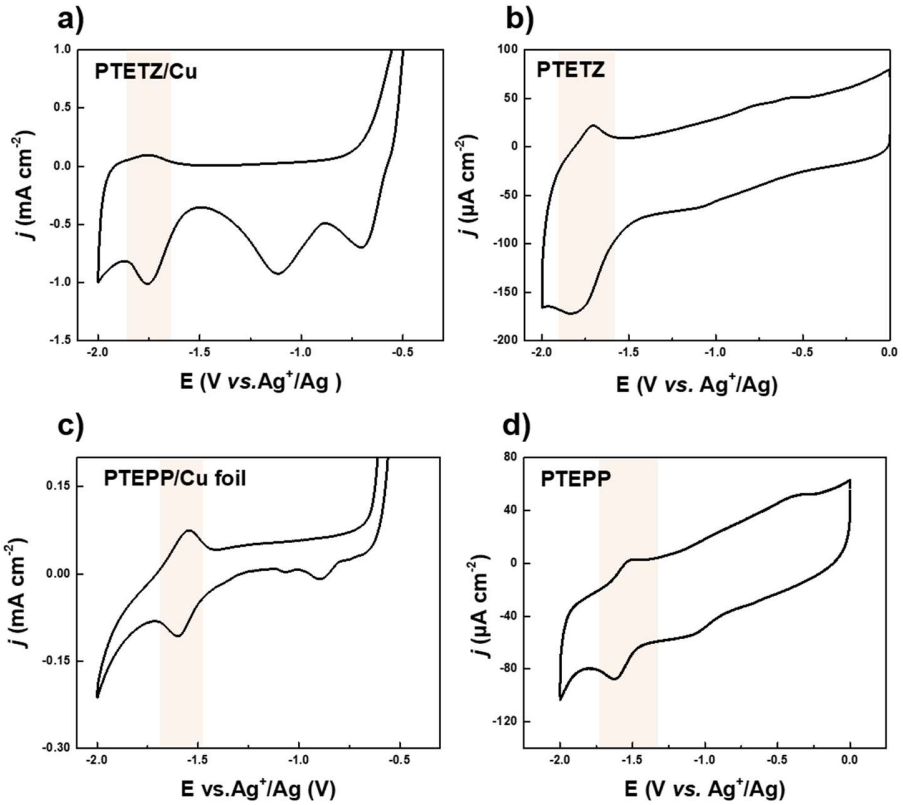

Figure S28. a) CV curves of PTETZ/Cu foil in N_2-saturated 0.1 M Bu_4NFP_6/CH_3CN. b) CV curves of TETZ polymer films on glass carbon electrode (GCE) in N_2-saturated 0.1 M Bu_4NFP_6/CH_3CN. PTETZ was obtained from 5S polycrystalline Cu foil (99.99%, with a thickness of 0.1 mm), which dropped during CO_2RR electrolysis (maybe because the PTETZ obtained from 5S Cu foil surface had no copper in the polymer layer, it would fall off easily during the electrolysis). c) CV curves of PTEPP/Cu foil in N_2-saturated 0.1 M Bu_4NFP_6/CH_3CN. d) CV curves of TEPP polymer films on glass carbon electrode (GCE) in N_2-saturated 0.1 M Bu_4NFP_6/CH_3CN. PTEPP was ultrasonically obtained from a thicker PTEPP/Cu foil, and treated with 1 M HCl.

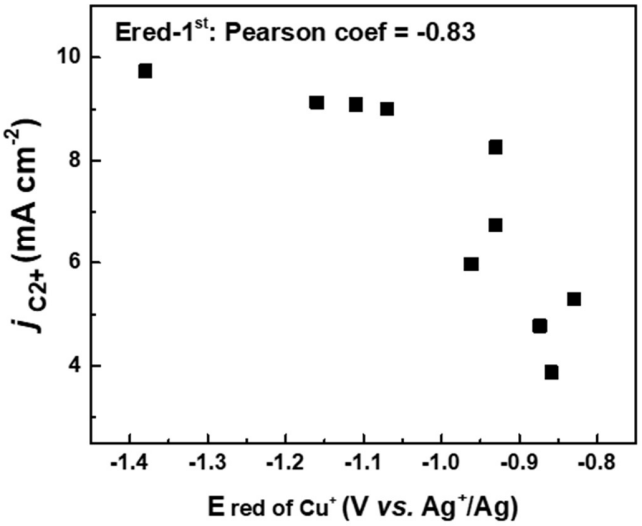

Figure S29. Relationship between the Cu^{+} reduction potential of polymer/Cu foils, Cu foil, py/Cu foil and corresponding partial curret density of C_{2+} (j C_{2+}).

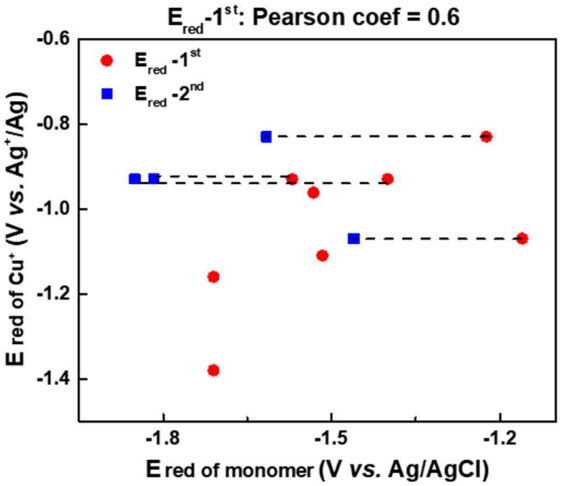

Figure S30. Relationship between the reduction potential of monomer and Cu^{+} reduction potential of polymer/Cu foil.

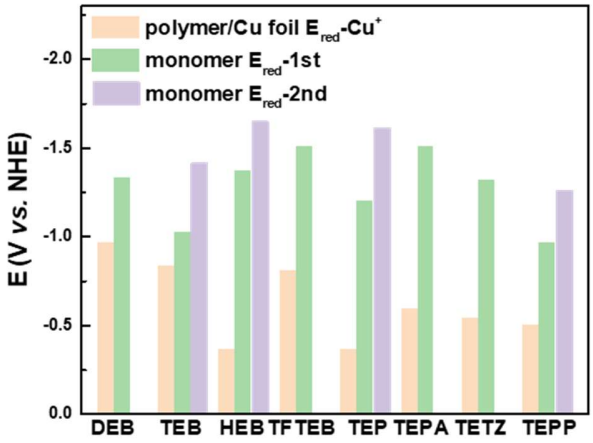

Figure S31 The second reduction potential of polymer/Cu foils and the corresponding reduction potential of monomers.

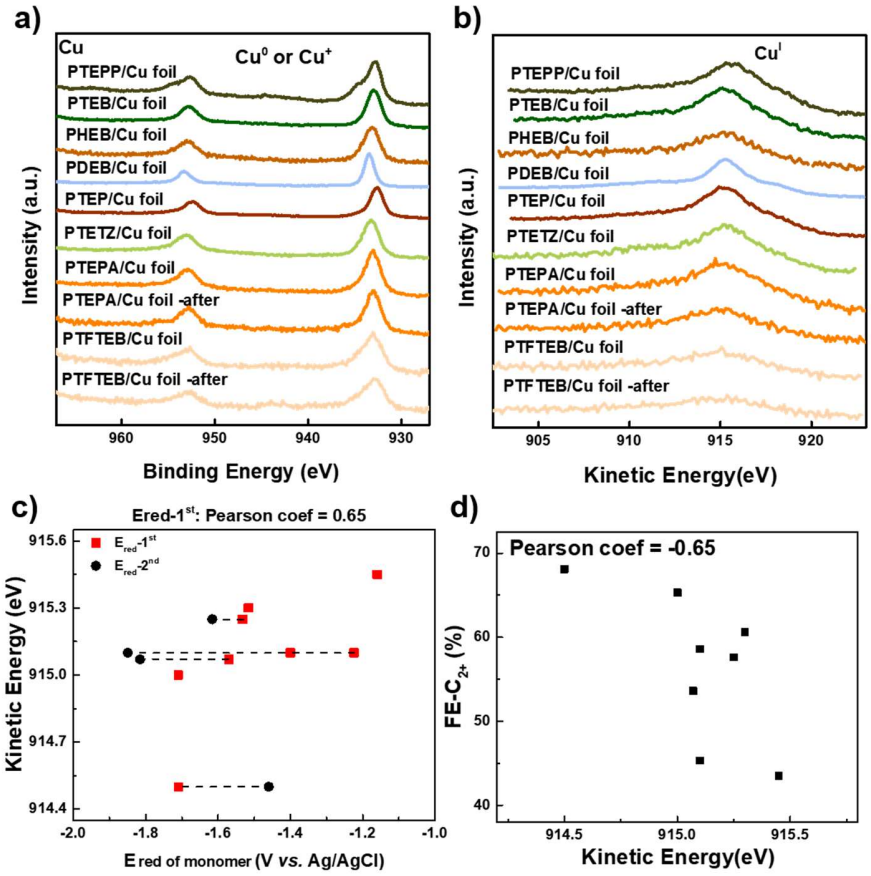

Figure S32. a) XPS spectra of Cu 2p for polymer/Cu foil before and after electrocatalytic CO_2 reduction, b) Auger electron spectra (AES) for the same samples. c) Relationship between the reduction potential of

monomers and kinetic energy of Cu^{+}. d) Relationship between the kinetic energy of Cu^{+} and C_{2+}-FE of polymer/Cu foil.

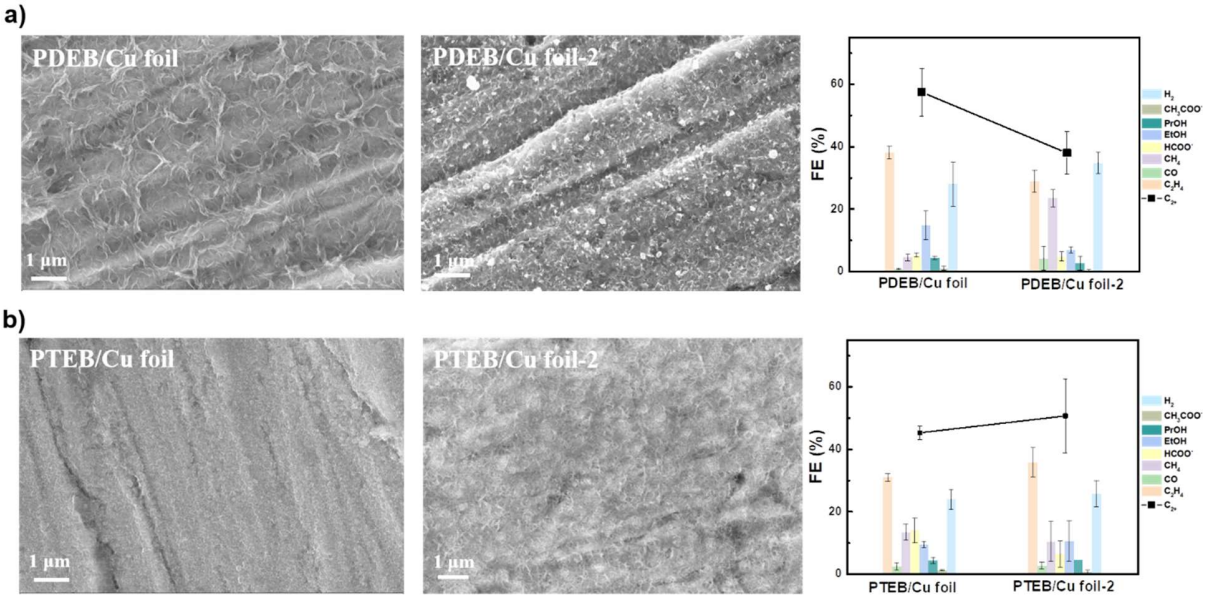

Figure S33. SEM images and CO_2RR performance of a) PDEB/Cu foil and b) PTEB/Cu foil synthesized by two precursors with and without TMS protection (denoted PDEB/Cu foil-2 and PTEB/Cu foil-2).

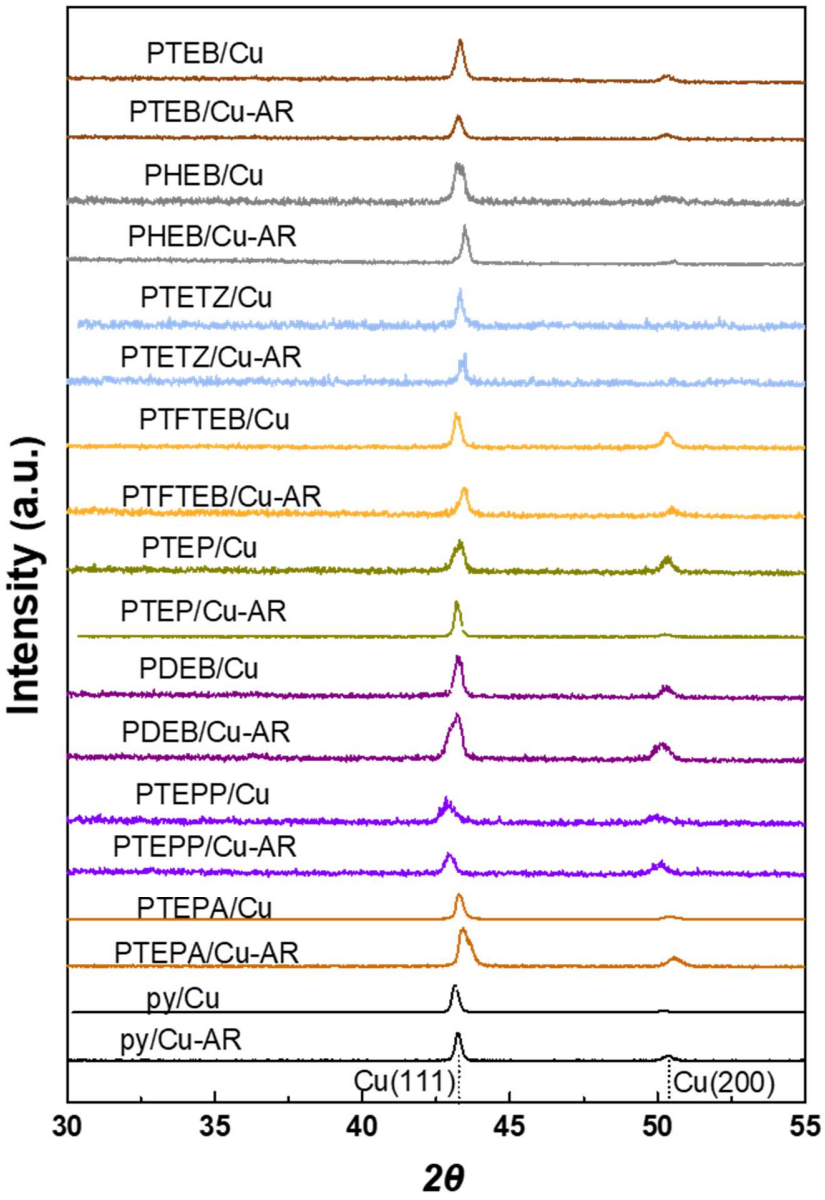

Figure S34. GIXRD pattern of polymer/Cu foil before and after electrocatalytic CO_2 reduction. The peak shift is affected by the height of the test gasket.

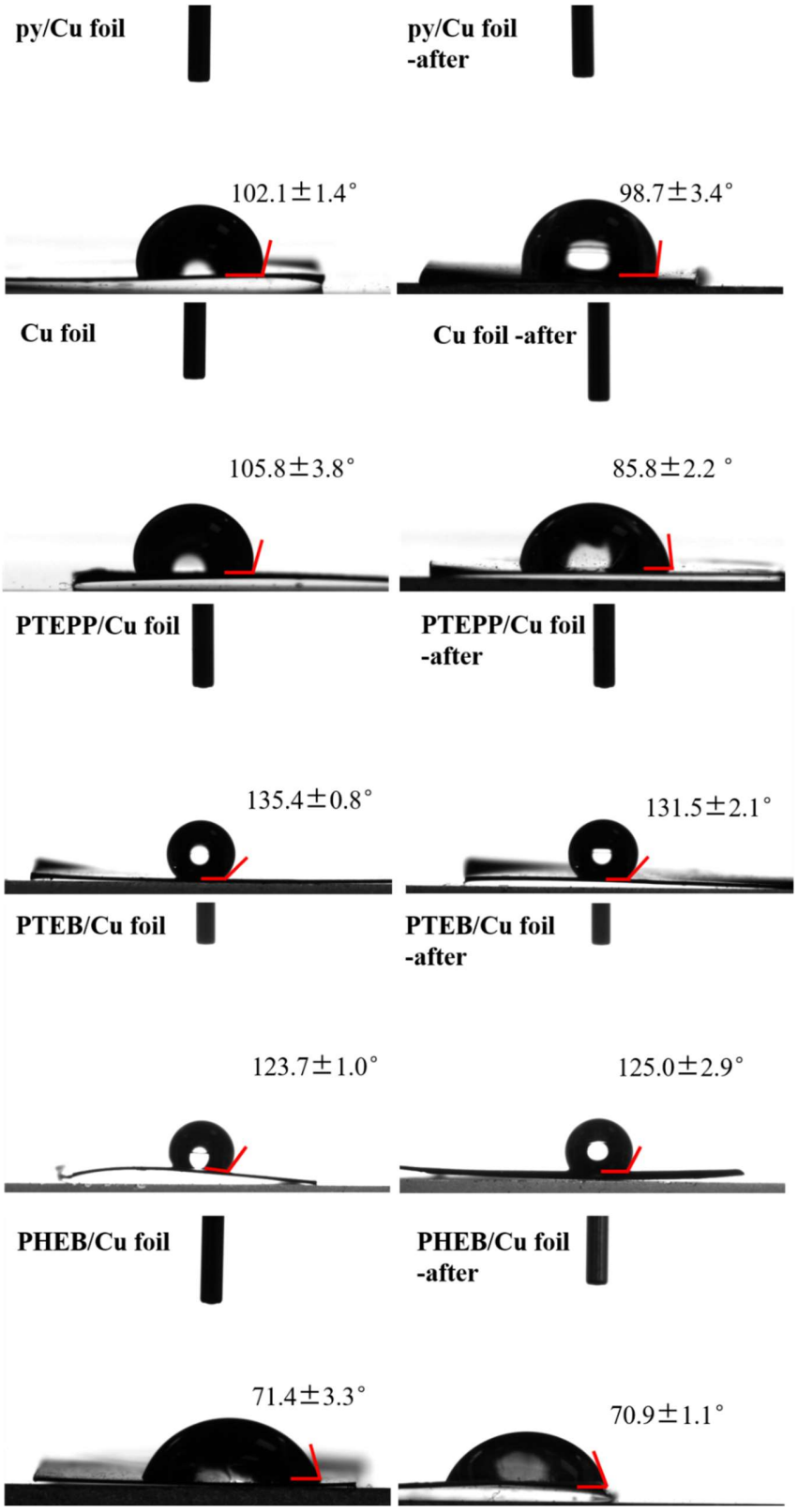
py/Cu foil
py/Cu foil -after
102.1±1.4°
98.7±3.4°
Cu foil
Cu foil -after
105.8±3.8°
85.8±2.2 °
PTEPP/Cu foil
PTEPP/Cu foil -after
135.4±0.8°
131.5±2.1°
PTEB/Cu foil
PTEB/Cu foil -after
123.7±1.0°
125.0±2.9°
PHEB/Cu foil
PHEB/Cu foil -after
71.4±3.3°
70.9±1.1°

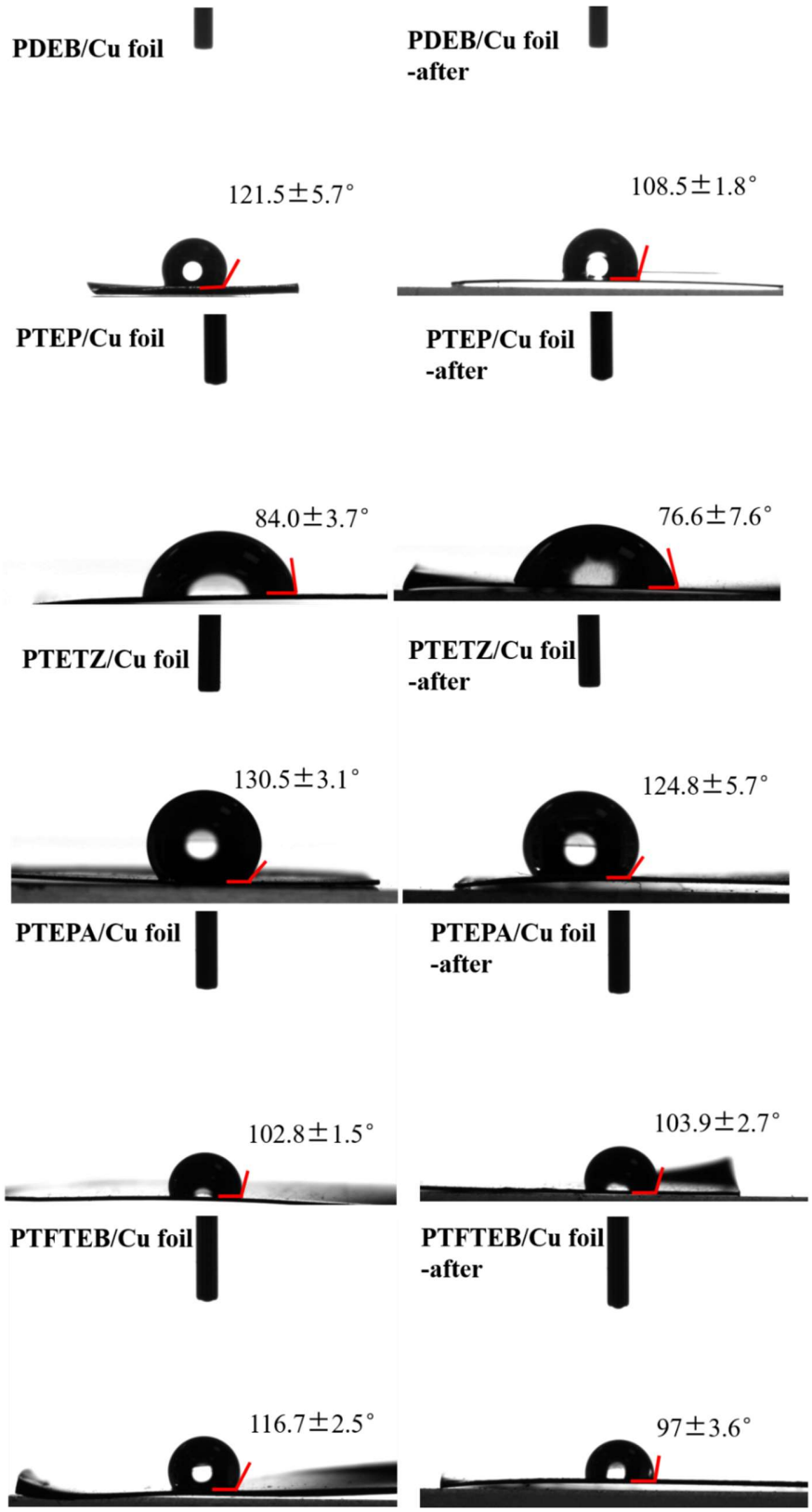

Figure S35. Photographs of contact angle measurements on polymer/Cu foil before and after electrocatalytic CO_2 reduction.

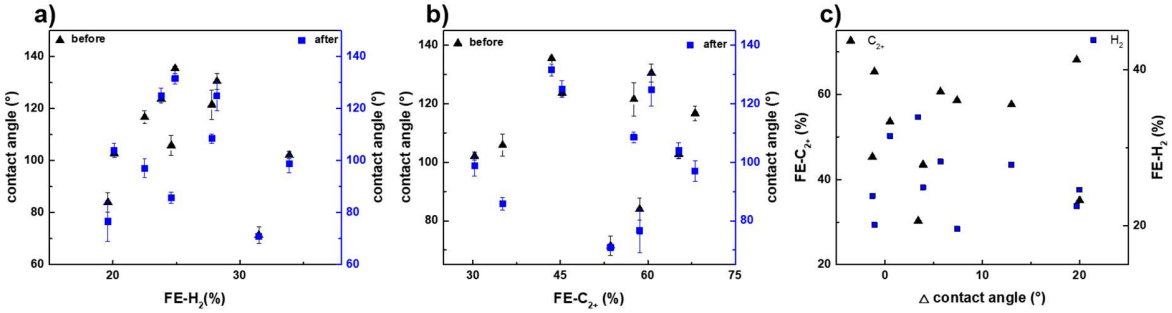

Figure S36. Relationship between contact angle, a) FE-H_2 and b) FE-C_{2+} on polymer/Cu foil before and after electrocatalytic CO_2 reduction. c) Relationship between the contact angle difference before and after electrolysis (Δcontact angle) and FE-C_{2+}, FE-H_2.

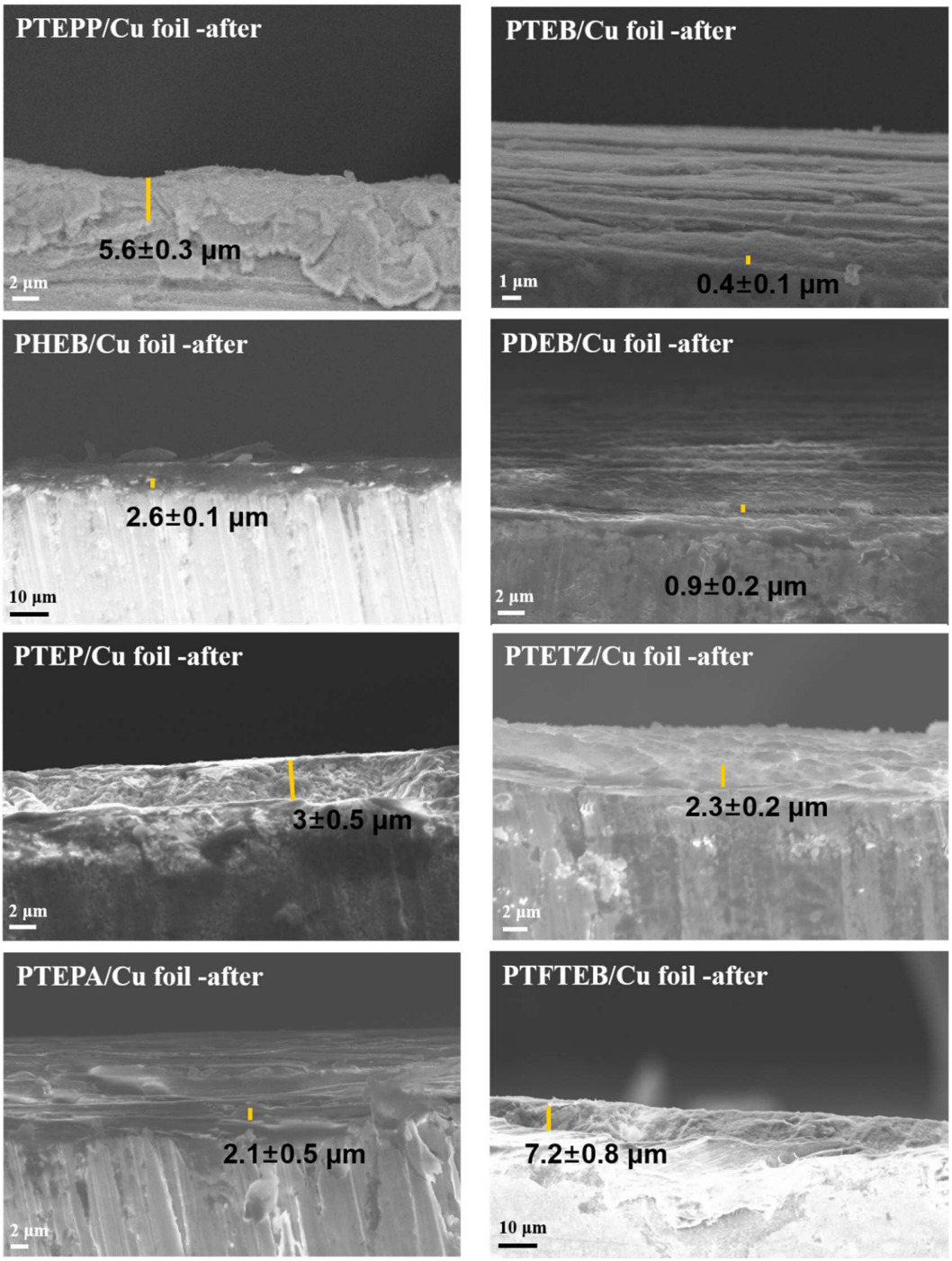

Figure S37. Cross section SEM images of polymer/Cu foil after electrocatalytic CO_2 reduction to measure the thickness of the polymer films.

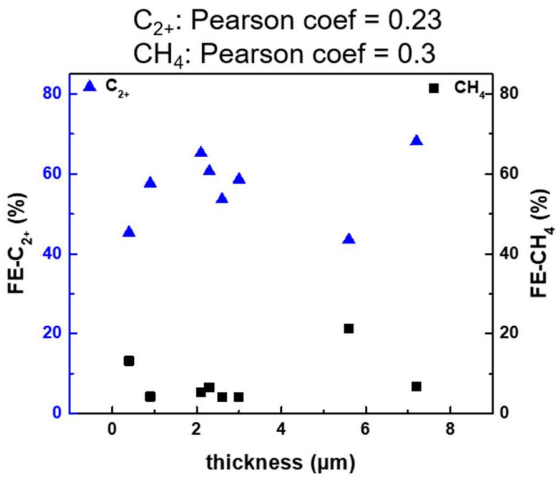

Figure S38. Relationship between polymer films thickness and FE-C_{2+}, FE-CH_4.

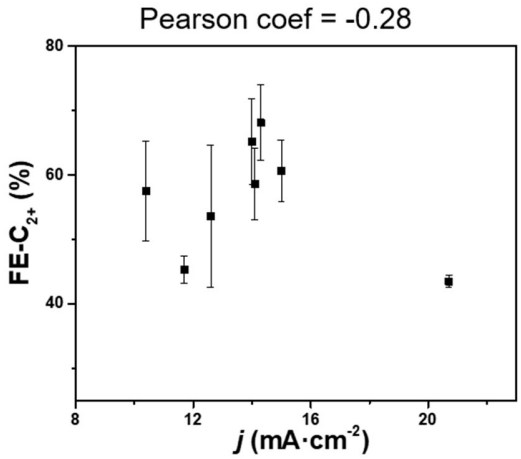

Figure S39. The correlation of current density of polymer/Cu foils and FE-C_{2+} for electrocatalytic CO_2 reduction.

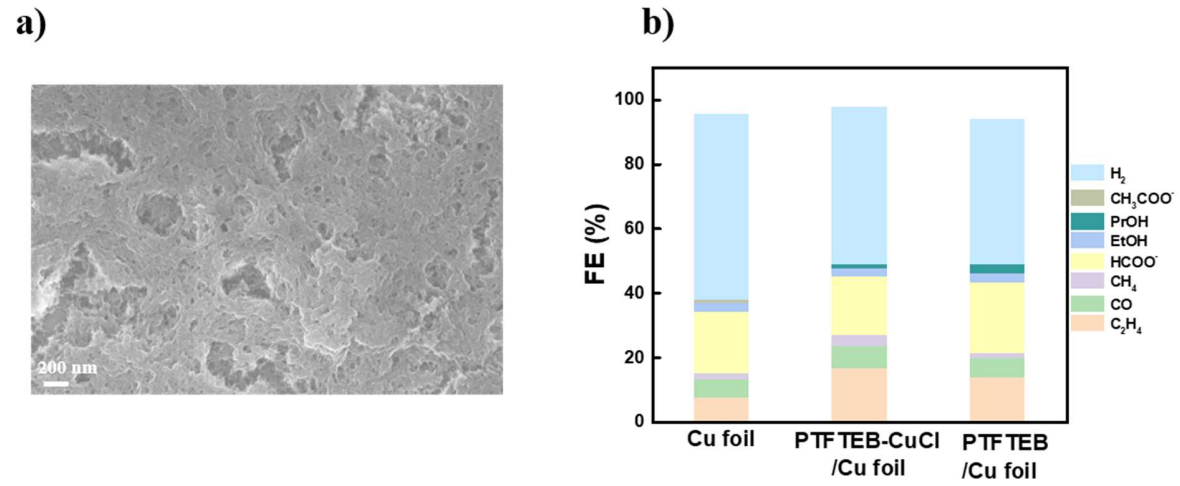

Figure S40. a) SEM images of PTFTEB-CuCl, b) Faradaic Efficiency (FE) of PTFTEB-CuCl/Cu foil, PTFTEB/Cu foil (PTFTEB-CuCl with 1M HCl treatment), and Cu foil at -1.2 V *vs.* RHE (without iR compensation).

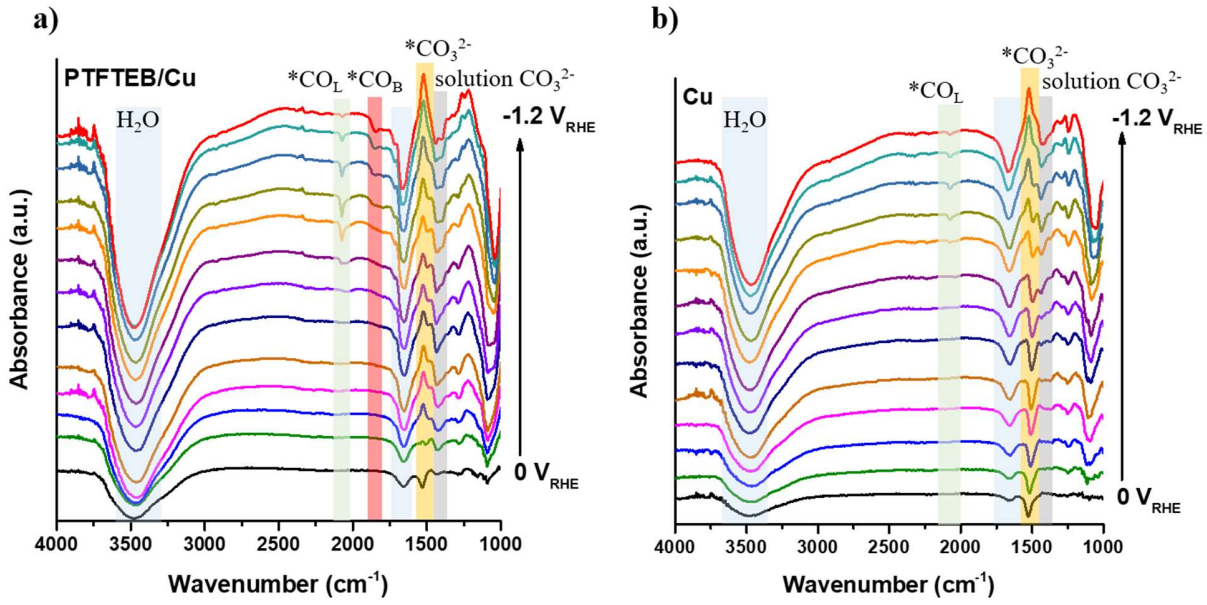

Figure S41. *In situ* ATR-FTIRS spectra of a) PTFTEB-CuCl on Cu film and b) Cu film in 0.1 M CO_2-saturated $KHCO_3$ (pH = 6.8) solution from 0 V to -1.2 V *vs.* RHE.

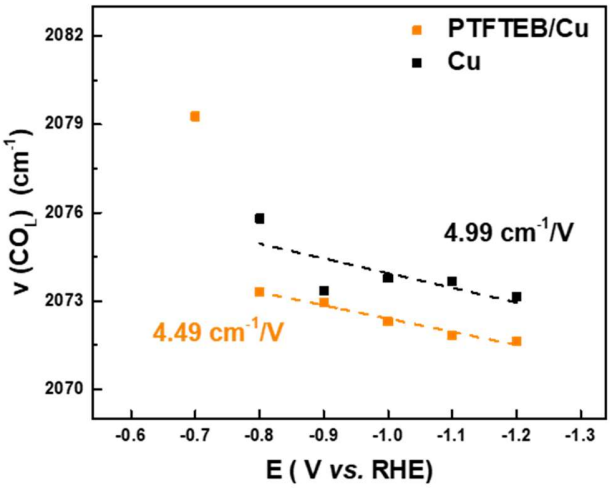

Figure S42. Stark effects of the linearly adsorbed CO (*CO_L) on Cu film and PTFTEB-CuCl on Cu film.

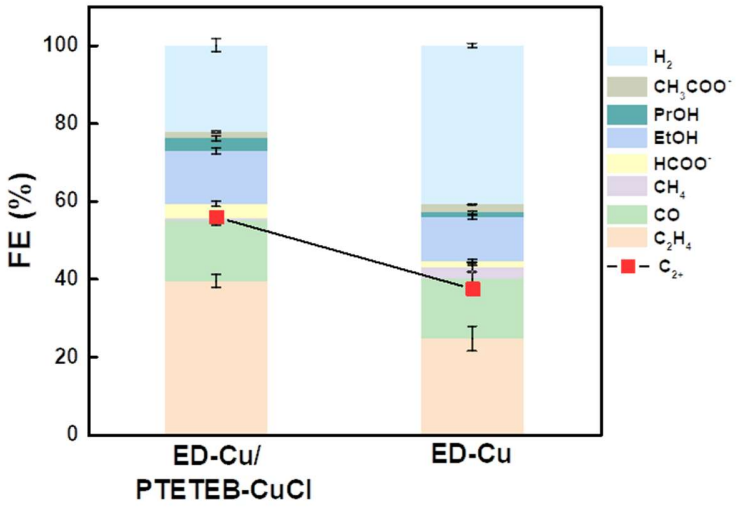

Figure S43. Faradaic Efficiency (FE) of electrodeposited Cu/PTFTEB-CuCl and electrodeposited Cu at -1.2 V *vs.* RHE in flow cell using 1 M KOH as the electrolyte.

References

1. M. Zhong, K. Tran, Y. Min, C. Wang, Z. Wang, C.-T. Dinh, P. De Luna, Z. Yu, A. S. Rasouli, P. Brodersen, S. Sun, O. Voznyy, C.-S. Tan, M. Askerka, F. Che, M. Liu, A. Seifitokaldani, Y. Pang, S.-C. Lo, A. Ip, Z. Ulissi and E. H. Sargent, *Nature*, 2020, **581**, 178-183.

2. X. Yan, C. Chen, Y. Wu, S. Liu, Y. Chen, R. Feng, J. Zhang and B. Han, *Chem. Sci.*, 2021, **12**, 6638-6645.
3. S. Zhen, G. Zhang, D. Cheng, H. Gao, L. Li, X. Lin, Z. Ding, Z. J. Zhao and J. Gong, *Angew. Chem. Int. Ed.*, 2022, **61**, e202201913.
4. W. Ma, S. Xie, T. Liu, Q. Fan, J. Ye, F. Sun, Z. Jiang, Q. Zhang, J. Cheng and Y. Wang, *Nature Catalysis*, 2020, **3**, 478-487.
5. Z. Li, Y. Yang, Z. Yin, X. Wei, H. Peng, K. Lyu, F. Wei, L. Xiao, G. Wang, H. D. Abruña, J. Lu and L. Zhuang, *ACS Catal.*, 2021, **11**, 2473-2482.
6. Z. Wang, Y. Li, X. Zhao, S. Chen, Q. Nian, X. Luo, J. Fan, D. Ruan, B.-Q. Xiong and X. Ren, *J. Am. Chem. Soc.*, 2023, **145**, 6339-6348.
7. F. Li, A. Thevenon, A. Rosas-Hernández, Z. Wang, Y. Li, C. M. Gabardo, A. Ozden, C. T. Dinh, J. Li, Y. Wang, J. P. Edwards, Y. Xu, C. McCallum, L. Tao, Z.-Q. Liang, M. Luo, X. Wang, H. Li, C. P. O'Brien, C.-S. Tan, D.-H. Nam, R. Quintero-Bermudez, T.-T. Zhuang, Y. C. Li, Z. Han, R. D. Britt, D. Sinton, T. Agapie, J. C. Peters and E. H. Sargent, *Nature*, 2020, **577**, 509-513.
8. Y. Zhao, L. Hao, A. Ozden, S. Liu, R. K. Miao, P. Ou, T. Alkayyali, S. Zhang, J. Ning, Y. Liang, Y. Xu, M. Fan, Y. Chen, J. E. Huang, K. Xie, J. Zhang, C. P. O'Brien, F. Li, E. H. Sargent and D. Sinton, *Nature Synthesis*, 2023, **2**, 403-412.
9. J. Wang, T. Cheng, A. Q. Fenwick, T. N. Baroud, A. Rosas-Hernandez, J. H. Ko, Q. Gan, W. A. Goddard, III and R. H. Grubbs, *J. Am. Chem. Soc.*, 2021, **143**, 2857-2865.
10. Y. Su, Y. Dai, Y. Zeng, C. Wei, Y. Chen, F. Ge, P. Zheng, D. Zhou, P. O. Dral and C. Wang, *Advanced Science*, 2023, **10**, 2204902.
11. G. Li, Y. Li, H. Liu, Y. Guo, Y. Li and D. Zhu, *Chem. Commun.*, 2010, **46**, 3256-3258.
12. C. Xing, Y. Xue, B. Huang, H. Yu, L. Hui, Y. Fang, Y. Liu, Y. Zhao, Z. Li and Y. Li, *Angew. Chem. Int. Ed.*, 2019, **58**, 13897-13903.
13. X. Xu, V. V. Jerca and R. Hoogenboom, *Macromol. Rapid Commun.*, 2020, **41**, 1900457.
14. M. I. Mangione, R. A. Spanevello and M. B. Anzardi, *RSC Advances*, 2017, **7**, 47681-47688.
15. Y. Tian, J. Wang, X. Cheng, K. Liu, T. Wu, X. Qiu, Z. Kuang, Z. Li and J. Bian, *Green Chemistry*, 2020, **22**, 1338-1344.
16. H. Huang, F. Li, Y. Zhang and Y. Chen, *J. Mater. Chem. A*, 2019, **7**, 5575-5582.